Tectonics®

RESEARCH ARTICLE
10.1029/2024TC008274

Salt Distribution in the South Pyrenean Central Salient: Insights From Gravity Anomalies

P. Santolaria[1], C. Ayala[2], R. Soto[3,4], P. Clariana[3,4], F. M. Rubio[5], J. Martín-León[6], E. L. Pueyo[3,4], and J. A. Muñoz[1]

[1]Departament de Dinàmica de la Terra i de L'Oceà, Facultat de Ciències de la Terra, Institut de Recerca Geomodels, Universitat de Barcelona (UB), Barcelona, Spain, [2]Geosciences Barcelona (GEO3BCN), CSIC, Barcelona, Spain, [3]Instituto Geológico y Minero de España, CSIC, Unidad de Zaragoza, Zaragoza, Spain, [4]Associated Unit in Earth Sciences - Universidad de Zaragoza-IGME (CSIC), Zaragoza, Spain, [5]Instituto Geológico y Minero de España, CSIC, Tres Cantos, Madrid, Spain, [6]Instituto Geológico y Minero de España, CSIC, Ríos Rosas, Madrid, Spain

Abstract Triassic evaporites represent the regional décollement of the Pyrenees and form two salt provinces north and south of the South Pyrenean Central Salient (SPCS). We present an updated Bouguer and residual Bouguer anomaly map built upon the homogenization of available gravity data of the SPCS together with four new and representative cross-sections, constrained by geological data acquired in the field, seismic, well, and gravity data (gravity forward modeling). Gravity anomaly maps and cross-sections are used to characterize the present-day uneven distribution of Triassic evaporites. Outcropping Triassic evaporites is not necessarily associated with an underlying evaporite accumulation and the absence of it at surface does not involves its non-existence at depth. Northwest of the salient, a major accumulation of Triassic evaporites floors a thick syn-orogenic Upper Cretaceous basin. South of it, Triassic rocks core salt-detached anticlines related to the Pyrenean orogeny. Along the southernmost (and youngest) thrust sheet of the salient, diapirs, and evaporite accumulations are associated with a salt-inflated area.

Plain Language Summary Gravity depends on the density of the rocks under our feet. In the South Pyrenean Central Salient (SPCS), an accurate measurement of gravity allows us to recognize gravity anomalies related to low density rocks, such as the Middle-Upper Triassic evaporites, and map their distribution. Among sedimentary rocks, evaporites have a particular behavior when deformed under geological forces: they flow. This characteristic determines a particular deformation style of the mountains. Characterize the present-day distribution of Triassic evaporites helps to reconstruct the geological history of the SPCS. Despite the apparent asymmetry of the salient, Triassic evaporites are unevenly distributed and specially accumulated to the northwest and southwest conforming evaporite inflated areas.

Key Points:

- Gravity anomalies help to assess the distribution of Triassic evaporites in the South Central Pyrenean Salient
- Seismically and gravity-constrained sections permit a further interpretation of gravity anomalies
- Inflated salt occurs mainly to the northwest and southeast of the salient, along the northernmost and southernmost thrust sheets

Correspondence to:

P. Santolaria,
p.santolaria.otin@ub.edu

Citation:

Santolaria, P., Ayala, C., Soto, R., Clariana, P., Rubio, F. M., Martín-León, J., et al. (2024). Salt distribution in the South Pyrenean Central Salient: Insights from gravity anomalies. *Tectonics*, *43*, e2024TC008274. https://doi.org/10.1029/2024TC008274

Received 24 JAN 2024
Accepted 17 APR 2024

Author Contributions:

Conceptualization: C. Ayala, R. Soto, P. Clariana
Formal analysis: C. Ayala, P. Clariana, F. M. Rubio
Investigation: C. Ayala, J. A. Muñoz
Methodology: C. Ayala
Project administration: C. Ayala, R. Soto, P. Clariana
Resources: F. M. Rubio, J. Martín-León, E. L. Pueyo
Validation: J. A. Muñoz
Writing – original draft: R. Soto, P. Clariana
Writing – review & editing: C. Ayala, R. Soto, P. Clariana, F. M. Rubio, J. Martín-León, E. L. Pueyo, J. A. Muñoz

1. Introduction

In fold-and-thrust belts, evaporites provide low strength units determining their structural style (e.g., Davis & Engelder, 1985; Izquierdo-Llavall et al., 2019; Letouzey et al., 1995). Their distribution is key to understand the width of fold-and-thrust belts and the presence and location of salients and reentrants (e.g., Bahroudi & Koyi, 2003; Luján et al., 2003). Thus, maps showing the distribution of evaporitic units represent a useful tool to understand factors controlling the architecture of salt-detached fold-and-thrust belts. Examples of such maps have been used to characterize deformation in the Zagros (Callot et al., 2012), Jura mountains (Hindle & Burkhard, 1999; Hindle et al., 2000) and the Monterrey salient (Wilkerson et al., 2007), for example. The influence of salt distribution during mountain building has been widely assessed using analog experimental models (e.g., Luján et al., 2003; Santolaria et al., 2024; Schreurs et al., 2001 and references therein). As a general rule, fold-and-thrust belts grow and expand mimicking the pre-deformation distribution of evaporites. Consequently, salients and reentrants form where there are and there are not evaporites, respectively, and transfer zones and oblique structures occur in between these domains (e.g., Bahroudi & Koyi, 2003; Schreurs et al., 2001). Yet, there are exceptions if salt pinch-outs appear at a certain angle to the shortening direction (Muñoz et al., 2024). However, in natural cases, the scarcity of subsurface information together with inherent limitations of the seismic method imaging salt units can hamper an accurate characterization of their distribution at depth. Gravity surveying can help overcome this problem due to its effectiveness in detecting anomalies produced by low-density rocks such as evaporites (e.g., Calvin et al., 2017; Nettleton, 1968; Pinto & Casas, 1996; Santolaria et al., 2016, 2020; Sarsar-

Naouali et al., 2011). Besides, it represents the bases for gravity forward modeling, a technique that provides an additional validation tool for geological cross-sections whose robustness has been largely proved in other salt provinces (AllahTavakoli et al., 2015; Jallouli et al., 2005; Pedrera et al., 2020; Ramos et al., 2022). Gravity forward modeling yields a quantitative interpretation of gravity anomalies and permits to interpret anomaly maps beyond their intrinsic qualitative character.

In the South Pyrenean Central Salient (SPCS) (i.e., historically referred as South-Pyrenean Central Unit; Séguret, 1972), the stratigraphic column is characterized by a basal pre-compressional evaporitic horizon, the Middle-Upper Triassic evaporites, and an intermediate syn-tectonic Eocene-Oligocene evaporitic layer deposited at the toe of this unit. Although the subsurface geometry of this salient has been elucidated from the interpretation of several 2D legacy reflection seismic profiles and wells (see Muñoz et al. (2018), and references therein), an accurate image of the distribution at depth of the Triassic and Cenozoic evaporites remains unsolved. Over the years, interpretations of the role played by evaporitic horizons in the configuration of the SPCS involve different degrees and combinations of thrust versus salt tectonic models (e.g., Burrel & Teixell, 2021; Muñoz, 1992; Santolaria et al., 2016; Saura et al., 2016; Teixell & Muñoz, 2000). Knowledge of the nowadays distribution of evaporites in the SPCS is key to propose an accurate structural and kinematic model for this salient.

During the past few years, some new densely sampled gravimetric surveys were focused on the SPCS and closer areas (Ayala et al., 2016; Ayala, Rey-Moral, Rubio, et al., 2021; Carrillo et al., 2020; Pueyo et al., 2021; Santolaria et al., 2016, 2020) and have provided more than 3,000 new gravimetric measurements. Gravity anomalies are here used to unravel the qualitative distribution of evaporitic horizons in the SPCS. In this work we present an updated and harmonized gravity anomaly of the SPCS together with four new and geophysically constrained N-S and W-E cross-sections that illustrate the architecture of this Pyrenean salient. These cross-sections not only help us delimiting the distribution and geometry of the salt horizons and salt structures at depth but provides further meaning to gravity anomalies which represent the foundation for the proposed salt distribution model of the area. We also discuss and compare this distribution with previous subsurface interpretations and its implication in shaping the SPCS.

2. Geological Setting

The Pyrenean mountain range formed as a WNW-ESE trending asymmetric, doubly verging wedge related to the convergence between the Iberian and European plates from Late Cretaceous to Early Miocene times (e.g., Roest & Srivastava, 1991; Roure et al., 1989). The Pyrenean thrust system incorporated Paleozoic rocks deformed during the Variscan Orogeny (e.g., García-Sansegundo, 1996; Poblet, 1991), Mesozoic successions sedimented in a rift to post-rift setting (García-Senz & Muñoz, 2019a, 2019b) and synorogenic sequences deposited during the Late Cretaceous-Cenozoic. In this work, we focus on the study of the SPCS, a major thrust salient located In the South-Central Pyrenees whose structural architecture has been studied for many years, authors and different approaches (e.g., Barnolas & Gil-Peña, 2001; Beamud et al., 2011; Choukroune & ECORS Team, 1989; Fillon et al., 2013; García-Senz, 2002; Garrido-Megías, 1973; Garrido-Megías & Ríos, 1972; Martínez Peña, 1991; Meigs & Burbank, 1997; Muñoz et al., 2013, 2018; Mutti et al., 1988; Nijman, 1998; Pocoví, 1978; Puigdefàbregas et al., 1992; Séguret, 1972; among many others). The SPCS was formed from North to South by the Bóixols-Cotiella, Peña Montañesa-Montsec, and Gavarnie-Sierras cover Thrust Sheets (e.g., Muñoz et al., 2013) (Figure 1) and emplaced following a predominantly foreland propagating thrust sequence from Late Cretaceous to Oligocene (e.g., Beaumont et al., 2000; Ford et al., 2022; Muñoz, 1992). It is characterized by a Cenozoic-Mesozoic cover succession detached from the Paleozoic rocks along the Upper Triassic evaporites, which represent the main detachment horizon (e.g., Muñoz, 1992; Muñoz et al., 2018; Vergés et al., 1992). Toward the South, it overthrusts the Cenozoic deposits of the Ebro Basin, which are found in the footwall of the Pyrenean sole thrust (e.g., Martínez-Peña & Casas-Sainz, 2003; Muñoz, 1992; Teixell & Muñoz, 2000; Vergés & Muñoz, 1990). The SPCS consists of Middle Triassic dolostones and limestones (Muschelkalk facies), Upper Triassic evaporites and shales (Keuper facies), thick sequences of Jurassic and Lower Cretaceous marine limestones and marls, Upper Cretaceous limestones, calcarenites, and marls, Paleocene-Eocene limestones, sandstones, marls and conglomerates and Oligocene-Neogene continental conglomerates and sandstones (e.g., Séguret, 1972).

Northwards of the SPCS, Paleozoic and Triassic rocks constitute a south-directed antiformal stack of basement thrust sheets forming the core of the range and referred to as the Axial Zone (Mattauer, 1968; Muñoz, 1992) (Figure 1). The uppermost basement thrust sheet (i.e., the Nogueras thrust sheet) has been refolded and its

10.1029/2024TC008274

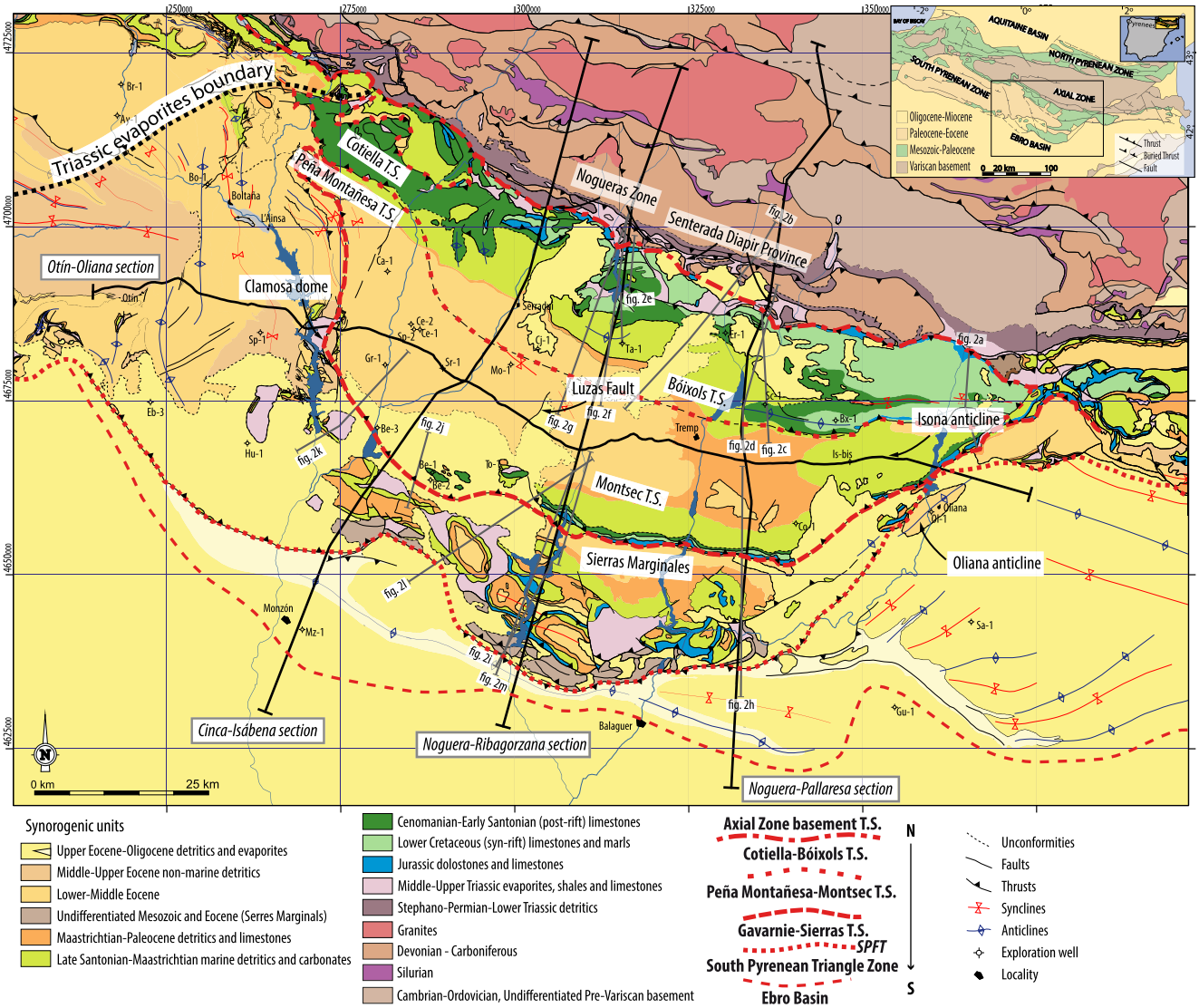

Figure 1. Geological map of the South Pyrenean Central Salient. Modified after Muñoz et al. (2013, 2018), Clariana et al. (2022), and Soto et al. (2022). Main structural units are limited by dotted/dashed red lines and labeled. Traces of gravity-constrained and previously published sections are shown in black to gray lines, respectively.

southern leading edge even shows downward facing structures (i.e., the so-called Nogueras Zone, Dalloni, 1913; Séguret, 1972). It is formed by upper Paleozoic rocks and Permian to Lower Triassic red beds (Figure 1) (Séguret, 1972). Two more basement thrust sheets crop out in the study area and two more younger basement thrust sheets have been interpreted at depth (e.g., Muñoz et al., 2018). The stratigraphy of the Axial Zone close to the SPCS varies largely in lithology and age spanning from Late Proterozoic to the Triassic. The pre-Variscan series are characterized by Cambro-Ordovician siliciclastic rocks with some intercalations of limestones and microconglomerates, Silurian black shales, Devonian slates and limestones and Carboniferous siliciclastic rocks. Late Carboniferous-Permian granites, volcanic and volcaniclastic rocks and Permian sandstones, shales and microconglomerates characterize the upper part of the Paleozoic succession (see e.g., García-Sansegundo et al., 2011). All these rocks have been metamorphosed during the Variscan orogeny and intruded by magmatic rocks (mainly granitoids) emplaced in a syn- to postcollisional setting during the Late Carboniferous-Early Permian (Aguilar et al., 2014).

The SPCS present two distinct salt provinces characterized by extensive outcrops of Triassic evaporites located: (a) along the contact between the Nogueras Zone and the Bóixols Thrust Sheet, and (b) inside the Gavarnie-Sierras cover Thrust Sheet (Figure 1). The first one features squeezed diapirs, some of them still preserved

10.1029/2024TC008274

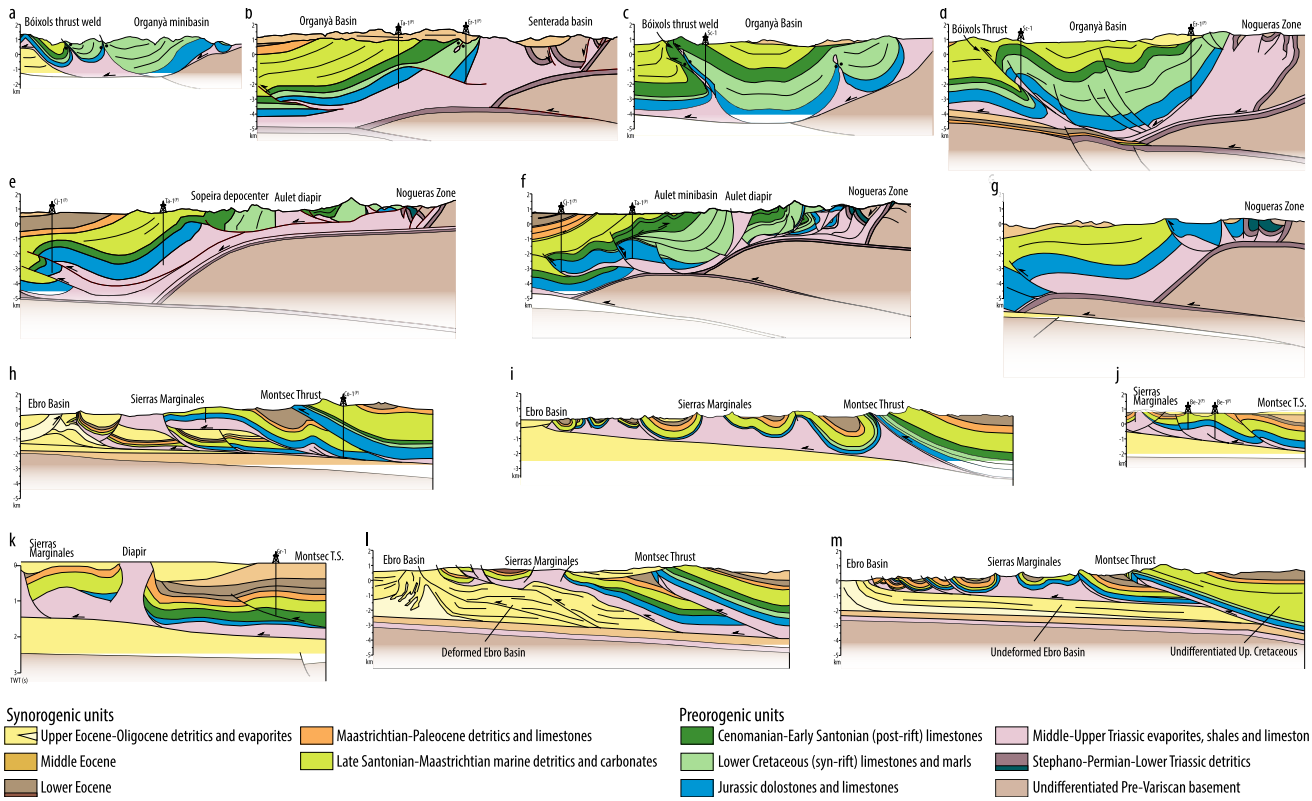

Figure 2. Some of the published sections along the South Pyrenean Central Salient that illustrate the along strike variability of the different structures but also the different interpretations of them. Modified after (a) Casini et al. (2023), (b) Burrel et al. (2021), (c) Casini et al. (2023), (d) Muñoz et al. (2018), (e) Saura et al. (2016), (f) Muñoz et al. (2018) and García-Senz and Muñoz (2019a), (g) Clariana et al. (2022), (h) Berástegui et al. (1993), (i) Burrel and Teixell (2021), (j) Gessal (2010) after Martínez Peña (1991), (k) Cámara and Flinch (2017), (l) Senz and Zamorano (1992), and (m) Martínez-Peña and Pocoví (1988). Trace lines are depicted in Figure 1.

and some others completely welded (e.g., García-Senz & Muñoz, 2019a; López-Mir et al., 2014; Saura et al., 2016) while the second one is characterized by deep- to shallow-seated diapirs and Triassic salt flooring thrust sheets. The distribution of Triassic evaporites at surface does not lead to a univocal interpretation of its distribution at depth and, over the years, different authors have proposed different interpretations of the continuation of Triassic bodies at depth and thus different volumetric distribution of these rocks (see Figure 2, e.g., Berástegui et al., 1993; Burrel & Teixell, 2021; Burrel et al., 2021; Cámara & Flinch, 2017; Casini et al., 2023; Clariana et al., 2022; García-Senz & Muñoz, 2019a, 2019b; Martínez-Peña & Pocoví, 1988; Muñoz et al., 2018; Saura et al., 2016; Senz & Zamorano, 1992; Teixell & Muñoz, 2000; Vergés, 1993). Thus, Figure 2 shows several geological cross-sections interpreting very different volumes (areas in section view) of Triassic evaporites at depth. The reasons of these important variations could be attributable to: (a) most wells do not reach the base of the Triassic evaporites to accurately draw the thickness of this unit (Lanaja, 1987), (b) ambiguity derived from non-resolute seismic interpretation when salt is present, (c) a lack of knowledge of the location of original Upper Triassic depocenters, and (d) an intricate syn-rift, post-rift and syn-orogenic migration history of Triassic evaporites and shales leading to abrupt across- and along-strike thickness variations (e.g., García-Senz, 2002; López-Mir et al., 2014, 2015; Martínez Peña, 1991; Muñoz et al., 2013, 2018; Santolaria et al., 2016; Saura et al., 2016 and many others).

3. Data and Methods

3.1. Gravity Data Processing, Bouguer Anomaly Calculation, Regional-Residual Separation

The gravity data we have used in this investigation comes from a compilation of available terrestrial gravity data acquired over the last 30 years (Ayala et al., 2016; Ayala, Rey-Moral, Rubio, et al., 2021 and references therein). Within the study area, the data set comprises 12,727 gravity measurements (Figure 3a) of which 3,048

10.1029/2024TC008274

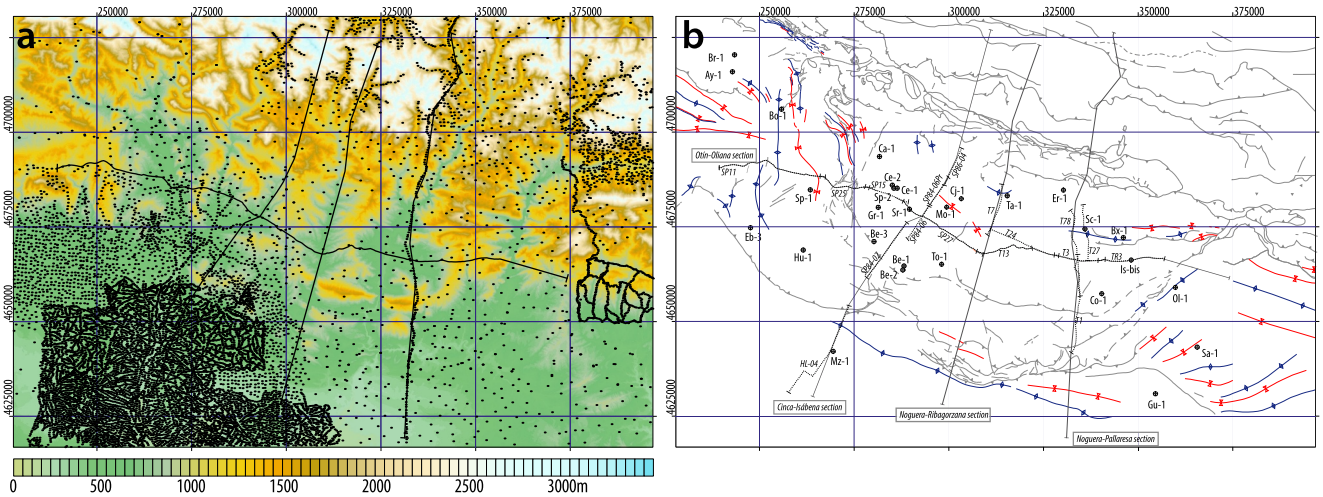

Figure 3. (a) Gravity measurements; contoured digital elevation model at the background. Digital elevation model has a resolution of 100 × 100 m and was built after the downsize of a merge of 25 × 25 m-resolution digital elevation model obtained from the Instituto Geográfico Nacional (Obra derivada de MDT25 2008–2015 CC-BY 4.0 ign.es). (b) Structural map of the South Pyrenean Central Salient with the location of the cross-sections (dark gray lines), exploration wells (encircled crosses, regular characters), and seismic reflection profiles used to constrain the cross-sections (dotted black lines, italic characters).

measurements were acquired in the past few years and led to a significant increase of the gravity resolution of the SPCS, from c. 1 measurement per 2–3 km^2 to c. 1 measurement per less than 1 km^2 (Ayala, Rey-Moral, Rubio, et al., 2021; Ayala, Rey-Moral, Rubio Sánchez-Aguililla, et al., 2021; Clariana et al., 2022; Santolaria et al., 2016, 2020; Soto et al., 2022). As described in the referred papers, all the measurements were taken with relative gravimeters (mainly Scintrex CG5 and Lacoste & Romberg, with an accuracy of 0.001 and 0.005 mGal respectively). Gravity measurements were carried out in itineraries with an estimated duration of less than 8 hr to minimize the effect of the instrument drift. At the end of each itinerary, the drift was corrected, and the tidal correction was applied (Longman, 1959; Rudman et al., 1977) prior to the Bouguer anomaly computation.

Since the gravity data came from different surveys, to obtain a homogeneous set of data, we recalculated the Bouguer anomaly using the Oasis Montaj v9 software that accounts for a Bouguer spherical cap of radius 166.7 km (LaFehr, 1991), that is, it accounts for the Earth curvature. For the calculation, we use the geodetic system GRS80 (Moritz, 1980) with orthometric heights, cartesian coordinates and with a reduction density of ρ = 2,670 kg/m^3. Given the size of the studied area (c. 110 × 170 km), terrain correction was applied up to 166.7 km, a standardized and recommended procedure for high-accuracy regional surveys that involve a broad range of elevations (Hinze et al., 2013), as it is the case for the Pyrenees. Yet, Fullea et al. (2008) demonstrate that to attain an accuracy of 0.1 mGal in the Bouguer anomaly calculation, the minimum distance required for the topographic correction even in rough areas is 20 km, so by calculating the topographic correction up to 166.7 km we ensure this accuracy. We have recalculated the topographic correction up to 166.7 km using an in-house software (CTT, Plata, 2014) based on the Hammer method. This method is based on calculating the gravity effect of a series of segmented annular rings (i.e., the Hammer chart, Hammer, 1939), centered around the measurement location. Each segment is called "zone." For this calculation we have used a DTM of 5, 25, and 200 m provided by the Geographical Institute of Spain, for zones A to M. These zones represent the inner terrain zones (distance up to 21.944 km from the measurement location) and require a more detailed DTM. For zones M to R, the outer terrain zone (distances from 21.944 to 166.7 km from the measurement location) we have used the regional Digital Elevation Model for Europe (EU-DEM) for the topography and European Marine Observation Data Network (EMDODnet) for the bathymetry. To generate the Bouguer anomaly grid displayed on the map in Figure 4a, Bouguer anomaly values were then interpolated using the kriging method with a grid spacing resolution of 1 km.

The resulting Bouguer anomalies (Figure 4a) are attributed to the combined effects of sources at various depths. In general terms, small and shallow bodies contribute to the short wavelength components and deep geological bodies contribute to the long wavelength components. The Bouguer anomaly of Figure 4a is characterized by a N120E gradient (ranging −120 to −25 mGal) with a variable slope that can be associated with the shallowing of

10.1029/2024TC008274

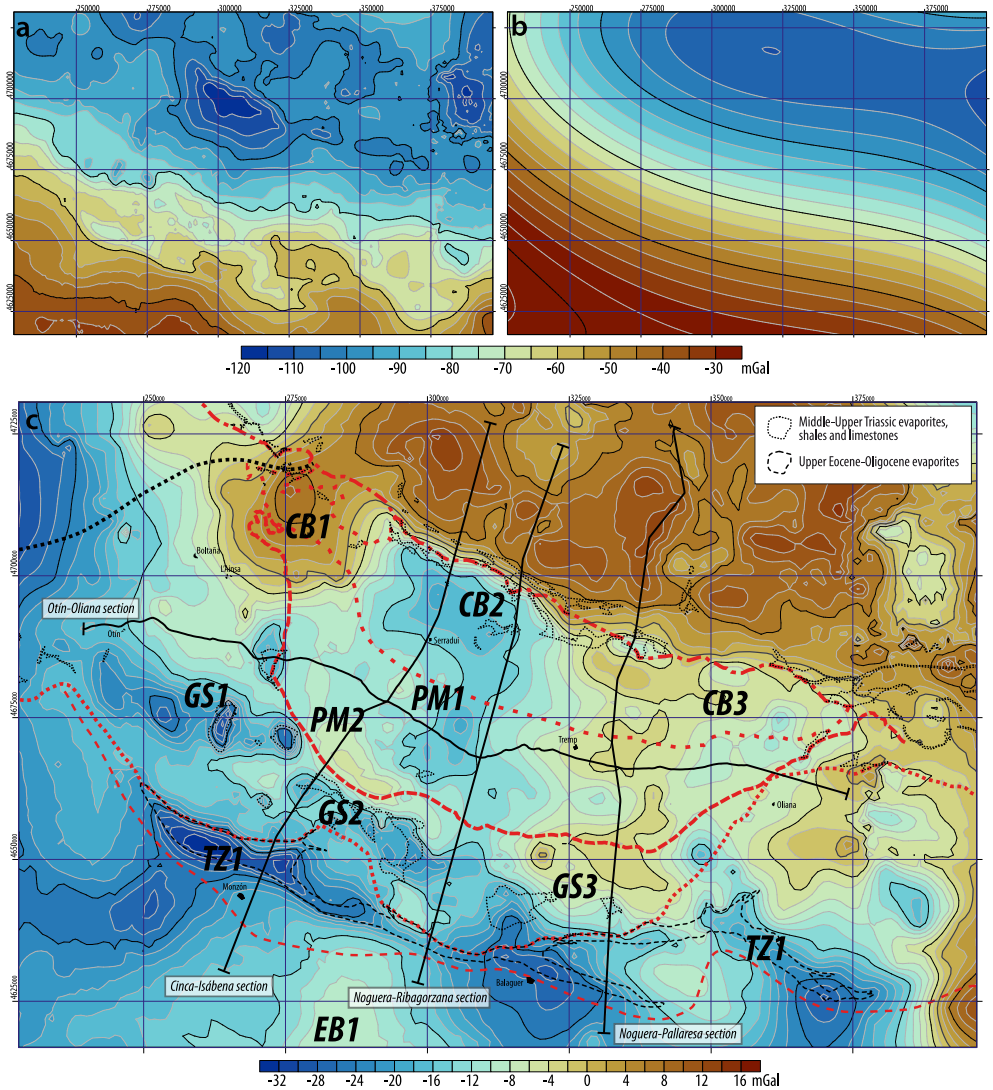

Figure 4. (a) Bouguer and (b) regional gravity anomaly maps (contour interval, 5 mGal). (c) Residual Bouguer anomaly map (contour interval, 2 mGal). Maps are colored using the Roma palette from Crameri (2018). Black lines are the section traces of the cross-sections. Red, dotted and dashed lines represent the boundaries of major geological units in the area (see legend in Figure 1). Black, dotted, and dashed lines represent the limits of Triassic and Eocene-Oligocene evaporites and shales. A thicker, dark-gray line represents the 0 mGal contour line, note that most of the positive values gather in the Axial Zone and in the northwestern tip of the Peña Montañesa-Montsec thrust Sheet.

the crust toward the Ebro Basin and a northern relative minimum plateau (−110 mGal) related to the contribution of the cortical root of the Pyrenees (e.g., Casas et al., 1997; Torné et al., 1989). Superimposed to this gradient and the minimum, some relative maxima and minima with variable amplitude (ranging from −115 to −45 mGal) and short to medium wavelength (ranging 2–3 km to more than 20 km) are shown. To model the uppermost part of the crust, we must separate out from the Bouguer anomaly the contribution of the deeper sources. We have tried several mathematical methods of regional-residual separation (isostatic, filtering, upward continuation, and polynomial fitting). We also performed power spectra analysis to estimate the depth of the source of anomalies but it was not conclusive. Such method assumes that long wavelength anomalies are related to deep-seated geological bodies. In our case both the Bouguer and the residual Bouguer gravity anomaly maps embrace long wavelength anomalies that are related to relatively shallow (<4 km) geological features associated with extensive accumulations of evaporites (e.g., Soto et al., 2022) or facies changes in the Ebro Basin (Santolaria et al., 2020). Power spectra analysis overestimates this kind of anomalies. Finally, after checking that the effect of the deep geological structures and crustal root had been removed, we have chosen as regional anomaly, a fourth-degree

polynomial. So, the residual Bouguer anomaly has been obtained by subtracting from the Bouguer anomaly a fourth-degree polynomial regional anomaly (Figure 4b). As stated in Ardestani et al. (2022), "the order of the polynomial depends on the complexity of the geology of the survey area and is mainly subject to the interpreter." This residual Bouguer anomaly is the one that is more consistent with the surface geology and reflects better the density distribution in the geological structures at the upper crust levels.

3.2. Geological Cross-Section Construction

Four new regional cross-sections (depicted by thick black lines in Figure 1) were constructed using available geological maps and data, alongside previous cross-sections (Berástegui et al., 1993; Muñoz et al., 2018; Saura et al., 2016; Teixell & Muñoz, 2000) and the interpretation of 16 seismic reflection legacy profiles. Similar to ours, previous cross-sections were also built upon field structural data, geological maps, mapping, and seismic interpretation. The total length of the seismic profiles amounts to about 280 km, representing approximately 60% of the entire length of the 4 cross-sections (Figure 3b). However, the seismic coverage is uneven, with most profiles running parallel to the Otín-Oliana and Cinca-Isabena cross-sections (Figure 3b). The seismic reflection profiles extend across the South Central Pyrenees, with none of them imaging the Axial Zone. The Sierras Marginales and sediments of the Ebro Basin underneath are generally poorly imaged, as is the deeper part of the Cotiella-Bóixols thrust sheet. The seismic profiles were reproduced at high-resolution (300 dpi) in TIFF format by scanning the original printed profiles. These scans were then cropped and imported into a 3-D environment software (MOVE) for their interpretation. Three of the cross-sections run perpendicular to the tectonic grain of the Pyrenees (i.e., N120E) and extend along the western, central and eastern parts of the SPCS. The fourth cross-section is approximately perpendicular to them and intersects with these sections.

Interpretation of seismic reflection profiles was constrained by nearby auxiliary intersecting seismic profiles and tied with exploration wells (Figure 3b). The lithological descriptions of the logs were synthesized by Lanaja (1987) and partially reinterpreted in different works (e.g., Mencos et al., 2015). The structural architecture was revisited through gravity forward modeling, especially in those parts of the cross-sections where seismic profiles do not successfully image the structure at depth, well data is not available, and surface geology preclude an unambiguous interpretation. Previous gravity forward models in this area include regional crustal-scale models of the western (Casas et al., 1997) and eastern (Torné et al., 1989) sides of the SPCS and smaller-scale models including the south-western (Santolaria et al., 2016, 2020) and south-eastern terminations (Torné, 1989) of the salient and the southern Axial Zone and the northern part of the salient (Clariana et al., 2022; Piña-Varas et al., 2023; Soto et al., 2022). Regional works tackled the overall crustal structure and therefore the scale of work differs from ours. Smaller-scale models were partially used but also reevaluated in our study.

3.3. Gravity Forward Modeling of the Cross-Sections

To refine the seismic interpretation, we have further constrained the geological cross-sections using forward gravity modeling with the residual Bouguer anomaly (Figure 4c) as the observed anomaly. In this technique, we model the gravity response of the cross-sections, where the geological units are characterized by specific densities. The modeling process is iterative, involving adjustments to the geometry of the cross-sections to ensure compatibility with the seismic sections while maintaining geological consistency. This iterative procedure continues until the calculated gravity anomaly for each cross-section matches the observed gravity anomaly. Density data used to perform the gravity forward modeling were derived from the analysis of over 2,000 rock samples collected and analyzed over the last 15 years in laboratories at IGME-CSIC and Zaragoza University (e.g., Clariana et al., 2022; Pueyo et al., 2022; Santolaria et al., 2016, 2020; Soto et al., 2022). These samples are representative of the lithological units represented in the cross-sections and ensure consistency across different cross-sections. A summary of the densities and corresponding lithologies is provided in Table 1. The density of Triassic rocks varies from 1.37 to 2.9 g/cm^3 because they include, in addition to salt, other evaporites such as gypsum or anhydrite, shales, marls, dolomites, carbonate breccias, and intrusive subvolcanic rocks known as "ophites" (Salvany & Bastida, 2004).

The calculations were carried out using the GM-SYS module, integrated into the Oasis Montaj® software developed by Geosoft. This module uses an algorithm based on the works of Talwani et al. (1959) and Won and Bevis (1987) to compute the gravity response of the corresponding density models. To avoid edge effects, the layers of each model were extended sufficiently beyond both ends of the profiles.

Table 1
Number of Samples (N), Mean, Mode, Standard Deviation, and Density Range Values for Each Geological Unit Used in This Study

Unit	*N*	Mean (g/cm^3)	Mode (g/cm^3)	SD	Range
Upper Eocene-Oligocene evaporites	163	2.22	2.28	0.13	1.84–2.64
Upper Eocene-Oligocene detritics (Ebro Basin)	588	2.37	2.42	0.19	1.28–3.04
Upper Eocene-Oligocene detritics (Pyrenean Cgs)	43	2.58	2.54	0.09	2.4–2.74
Middle-Upper Eocene non-marine deposits	148	2.64	2.68	0.1	2.47–3.23
Middle Eocene	93	2.59	2.63	0.1	2.33–2.8
Lower Eocene	236	2.55	2.62	0.09	1.93–2.77
Lower Eocene-Alveolina Fm.	37	2.67	2.7	0.05	2.39–273
Maastrichtian-Paleocene	31	2.67	2.65	0.2	2.23–3.63
Up. Cretaceous turbidites	15	2.56	2.69	0.11	2.34–2.69
Upper Cretaceous limestones	90	2.66	2.7	0.06	2.46–2.71
Jurassic Lower-Cretaceous	52	2.58	2.65	0.19	2.27–2.78
Middle-Upper Triassic evaporites, shales and limestones	147	2.3	2.26	0.2	1.37–2.9
Estefano-Permian-Lower Triassic detritics	99	2.59	2.64	0.17	1.85–2.89
Granites	98	2.66	2.65	0.08	2.29–2.9
Devonian-Carboniferous	90	2.7	2.69	0.1	2.41–3.03
Silurian	29	2.45	2.44	0.19	2.04–2.74
Cambrian-Ordovician	75	2.67	2.68	0.08	2.35–2.81

Given the well-constrained density values derived from the laboratory measurements, adjustments to observed anomalies were made basically by maintaining fixed mean densities and modifying depth geometries in regions with limited subsurface data. Where maintaining the mean density with a suitable geometry was not feasible, density values were adjusted within the range of the petrophysical data (Table 1). The root mean square fitting error, representing the difference between calculated and observed anomalies, ranged from 0.8 to 1.3 mGal across all the cross-sections. Notably, this error accounted for less than 5.3% of the observed anomaly amplitudes.

4. Residual Bouguer Anomaly and Gravity-Constrained Cross-Sections

4.1. Observed Residual Bouguer Anomaly

Observed residual Bouguer anomalies range from −34 to 14 mGal (Figure 4c). The gravity signal in the Axial Zone is characterized by a dominant gravity maximum with relative minima coinciding with the outcrop of Late Paleozoic granitoids or with buried granitoids and gneiss (Ayala, Rey-Moral, Rubio, et al., 2021; Ayala, Rey-Moral, Rubio Sánchez-Aguililla, et al., 2021; Clariana et al., 2022; Soto et al., 2022). This large-scale regional maximum can be associated with the usually higher density of Paleozoic rocks in the NE Iberian setting (Izquierdo-Llavall et al., 2019; Pueyo et al., 2016; Toro et al., 2021) and the antiformal stack of the Axial Zone.

In general, the eastern half of the SPCS displays higher gravity values compared to the western half. This along-strike asymmetry is overprinted by several lower wavelength anomalies as described below. The Cotiella-Bóixols Thrust Sheet shows a 40 km-long and 22 km-wide minimum (−18 mGal, Figure 4c, labeled CB2, Ayala, Rey-Moral, Rubio, et al., 2021; Ayala, Rey-Moral, Rubio Sánchez-Aguililla, et al., 2021; Clariana et al., 2022; Soto et al., 2022). This minimum does not have a direct correlation with cropping out rocks but is likely related to low density rocks in the subsurface. This low has a gravity gradient that is steeper to the north, along the contact with the Axial Zone, than to the south. To the west, it is flanked by a prominent maximum (7 mGal, Figure 4c, labeled CB1) that coincides with the western termination of the Cotiella-Bóixols and Peña Montañesa-Montsec Thrust Sheets. Toward the east, gentle gravity highs and lows occur (Figure 4c, labeled CB3, Ayala, Rey-Moral, Rubio, et al., 2021; Ayala, Rey-Moral, Rubio Sánchez-Aguililla, et al., 2021; Soto et al., 2022). In this area, gravity lows extend along the contact with the Axial Zone, where Middle-Upper Triassic evaporites, shales and carbonates are exposed (Figure 1). Gravity values ranging from −6 to 0 mGal dominate along the Peña

Montañesa-Montsec Thrust Sheet, except for a N-S oriented gravity low (−16 mGal, Figure 4c, labeled PM1) protruding from the prominent minimum to the north (CB2, Figure 4c). The location and orientation of this anomaly coincides with the Luzas Fault, a NNE-SSW trending fault that truncates Graus-Tremp Basin deposits (Figure 1). Adjacent and parallel to the southwestern contact between the Peña Montañesa-Montsec and Gavarnie-Sierras Thrust Sheets, an elongated, relative high appears (−5 mGal, Figure 4c, labeled PM2). Northwest of it, a N-S gravity low (−17 mGal) corresponds to the Clamosa Dome, a Triassic evaporite-cored diapir (Figure 1). To the south, the Gavarnie-Sierras Thrust Sheet is characterized by alternating gravity highs and lows. Here, the western gravity lows are constantly spaced, aligned WNW-ESE and correlate with diapirs or anticlines cored by Triassic evaporites (Figures 1 and 4c, labeled GS1) (Santolaria et al., 2016, 2020). The eastern gravity lows broadly coincide with outcrops of Triassic evaporites (Figures 1 and 3c, labeled GS2). The eastern part of this thrust sheet is characterized by a prominent 30 km-long and 16 km wide gravity high that could be associated with medium to high density rocks (Figure 4c, labeled GS3). Along the frontal South Pyrenean Triangle Zone, elongated gravity lows correlate well with anticlines or antiformal stacks cored by Eocene to Oligocene evaporites (Figures 1 and 4c, labeled TZ1, e.g., Pinto et al., 2002; Santolaria et al., 2020). South of it, the Ebro Basin gravity signal is characterized by tens of kms-wide highs (as for example EB1, in Figure 4c) and lows related with changes in the basement relief as well as lateral density changes within the sediments (Santolaria et al., 2020).

4.2. Gravity-Constrained Cross-Sections of the South Pyrenean Central Salient

Along the Noguera-Pallaresa section (Figure 5a), the residual Bouguer anomaly shows a wide gravity high in the Axial Zone antiformal stack attributed to the distribution of granitic bodies and Cambro-Ordovician to Devonian rocks. These geological units are, in general terms, denser than most of the units south of the Axial Zone (note that the influence of the crustal root of the Pyrenees has been removed during the gravity regional-residual separation). To the south, at the front of the Nogueras Zone, a 5 km-wide and 2.5 km-deep accumulation of Middle and Upper Triassic evaporites and shales produces a prominent gravity minimum (Figure 5a, labeled CB3). South of it, the Cotiella-Bóixols Thrust Sheet depicts a syncline geometry tipped to the south by the St. Corneli Anticline that resulted from the inversion of a Lower Cretaceous extensional fault system (Mencos et al., 2015). The observed gravity anomaly points to low volumes of evaporites below the synform except for a limited accumulation of them in the footwall of the Bóixols Thrust. The Montsec Thrust Sheet includes a gently folded Jurassic to Paleocene succession that ramps up along the south-directed Montsec thrust. In its footwall, a Lower Eocene depocenter overlies a reduced Jurassic to Paleocene succession that thins southwards. The Sierras Marginales unit, belonging Gavarnie-Sierras Thrust Sheet, is characterized by a complex set of frontal imbricates and out-of-sequence thrusts (Millán et al., 2000; Muñoz et al., 2018). A ca. 14 km-long gravity high (Figure 5a, labeled GS3) embraces the northern Sierras Marginales unit. South of it, observed gravity steadily declines in agreement with the decrease and thinning of the Mesozoic succession at expenses of the upper Eocene-lower Oligocene synorogenic sediments. The three observed minimum coincide with salt structures, the northern ones involving Triassic evaporites and the southern ones coinciding with anticlines cored by Eocene-Oligocene evaporites in the South Pyrenean Triangle Zone (e.g., Figure 5a, labeled TZ1).

In the northernmost part of the Noguera-Ribagorzana section (Figure 5b), the residual Bouguer anomaly depicts a northwards decreasing trend interrupted by a c. 2.3 km-wide relative maxima. This decreasing trend is attributed to the presence of the Maladeta and Artiés granitoid bodies (Clariana et al., 2022), with the Maladeta batholith comprising two distinct granitoid bodies as evidenced by gravity and magnetotelluric data (Piña-Varas et al., 2023). Southward, a gravity plateau correlates with the southern Axial Zone, dominated by heavily folded Devonian rocks. Similarly to the eastern section, the uppermost thrust sheet (Nogueres Zone) is folded and tilted (Muñoz, 1992). To the south, beyond the limit between the Axial Zone and the SPCS, gravity values decrease from 7 to −13 mGal in just 5 km. From there to c. 20 km to the south, gravity values depict a nearly flat anomaly featuring long-wavelength (4–7 km long) anomalies ranging from −12 to −15 mGal. Despite its apparent simplicity, this anomaly is sourced in a complex geological scenario (Figure 5b). It is worth noticing that this section cuts through the western edges of two significant gravity lows (CB2 and PM1) and a gravity low corridor that separates two gravity highs aligned along the Montsec thrust (Figure 4c). This last one is an area with no gravity measurements (Figure 2a) so gravity anomalies there should be taken cautiously. The Bóixols Thrust Sheet depict several km-thick Cretaceous depocenters, including the ∼4 km Sopeira Albian-Coniacian depocenter (Figure 5b) separated by preserved but laterally welded diapirs (e.g., Aulet diapir) (Saura et al., 2016). A problem

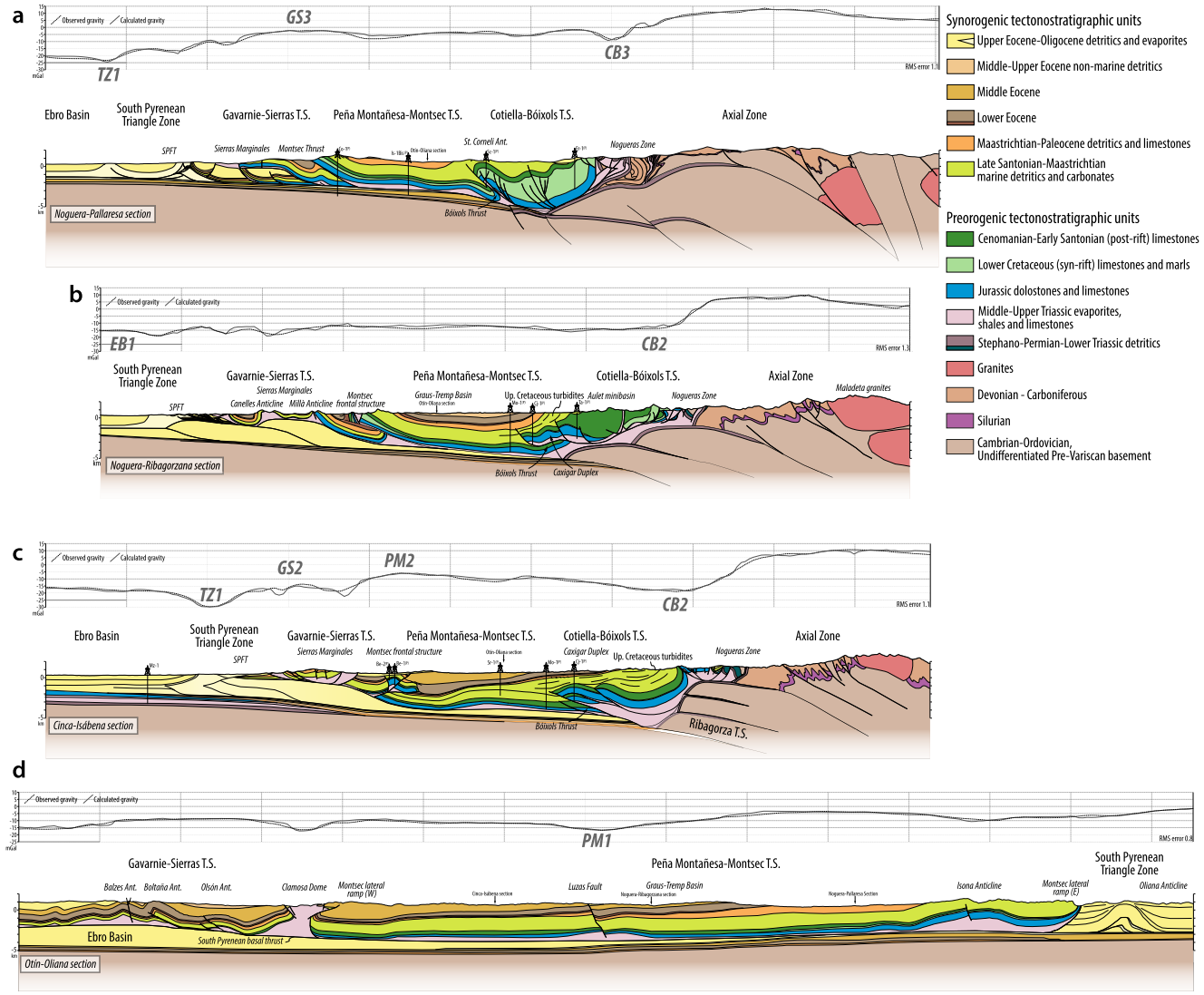

Figure 5. (a) Noguera-Pallaresa, (b) Noguera-Ribagorzana, (c) Cinca-Isábena, and (d) Otín-Oliana seismically and gravity-constrained sections. Location of sections are shown in Figures 1, 3, and 4 to facilitate their correlation with surface geology, the data sets that support their interpretation and the residual Bouguer anomaly, respectively.

lies on the nature of the structural units between the bottom of these minibasins and the sole thrust located at about 5–6 km underneath to explain the gravity anomaly. The structural relief has been resolved by two stacked basement-involved thrust sheets. In the section, we have interpreted the existence of a preserved inflated salt area underneath the Cretaceous minibasins (Figure 5b). However, this interpretation would be in contradiction with the laterally shifted depocenters of the minibasins that suggest primary welding (Gannaway et al., 2022; Saura et al., 2016). Alternatively, Permian basins involved into the basement thrust sheet and thinner Keuper evaporites above would also explain the gravity anomaly. These Permian sediments would be consistent with observed reflectors in the available seismic line close to the northern part of the section. At the southern tip of this accumulation of Triassic evaporites, the Caxigar duplex system (Figure 5b) represents the frontal structure of the Bóixols Thrust Sheet. To the south, the Graus-Tremp Basin synclinorium detached along a c. 350 m-thick Triassic evaporites décollement. A subtle, long-wavelength relative gravity low points out to the existence of a triangular-shaped accumulation of Triassic evaporites in the footwall of the Montsec thrust. South of the Montsec thrust front, gravity values decrease a mean of c. 3 mGal. Thus, there is not a significant drop of the gravity signal from the Montsec Thrust Sheet/Graus-Tremp Basin to the south as it occurs to the eastern and western sections (Figures 5a and 5c). To fit the modeled gravity signal with the observed anomaly, relatively denser Ebro Basin

deposits are needed. This is in good agreement with the N-S gravity high observed in the Ebro Basin (Figure 5b, labeled EB1). A series of c.5 km-wide, 5 mGal of amplitude, gravity highs and lows characterized the gravity signal of the Sierras Marginales and Ebro Basin. They correspond to Triassic salt accumulations in the Sierras Marginales and Barbastro-Balaguer salt cored anticline. In the Sierras Marginales, south of the Montsec, there are two prominent anticlines. The northernmost one (Millà anticline) is cored by a complete Jurassic succession, whereas the southern one (Canelles anticline) is cored by Triassic evaporites overlain by a reduced and thinned lowermost Jurassic or Upper Cretaceous carbonates. Such difference is shown by the negative gravity anomaly along the Canelles anticline (Figures 4 and 5b).

In the Cinca-Isábena section (Figure 5c), the Axial Zone consists of several north-dipping, south-directed basement thrust sheets. As in previous sections, the Nogueras Zone represents the tip of a folded and tilted basement thrust sheet (Muñoz, 1992). In the Axial Zone, the observed residual Bouguer anomaly shows a relative gravity maximum that gently decreases to the south where it rapidly drops from 5 to −18 mGal in the contact between the Axial Zone and the Cotiella-Bóixols Thrust Sheet. In this zone Triassic evaporites crop out and have been interpreted at depth, running parallel to the tips of basement thrust sheets. Triassic evaporites continue and thicken to the south as evidenced by a tens of kms-wide gravity low (Figure 5c, labeled CB2). This evaporite accumulation is here interpreted to sole the Cotiella-Bóixols Thrust Sheet. The Cotiella-Bóixols Thrust Sheet forms a 6 km wide syncline whose southern limb included a set of duplexes and imbricates that represents the hanging wall of the Bóixols Thrust (Muñoz et al., 2018). Growth of this structure was coeval with the deposition of late Santonian to Campanian, syn-inversion turbidites (Ardèvol et al., 2000; Van Hoorn, 1971), showing two depocenters at both sides of the Bóixols frontal structure (Figure 5b). Few km to the south, the Mesozoic succession forms a gentle, salt-cored detachment anticline, drilled by the Santa Creu well, coinciding with a gravity low. To the south, gravity values increase and culminate in a prominent relative maximum (−6 mGal, Figure 5c, labeled PM2). This gravity high points to the absence of a significant accumulation of Triassic evaporites despite being drilled by the Benabarre-1 (Be-1) exploration (Top, −700 m.b.s.l). This well also drilled Hettangian-Sinemurian anhydrites and dolostones (Top, −213 m.b.s.l.), dense rocks (2.9 g/cm^3) that slightly contribute to this gravity high due to their limited distribution and thickness. This gravity high corresponds to the frontal structure of the Montsec Thrust which, unlike to the eastern sections, is characterized by a pop-up structure bounded, to the north, by a backthrust and, to the south, by an inverted pre-existing extensional fault. This structure ramps up over the Ebro Basin autochthonous deposits. To the south, a reduced and southward-thinning Upper Cretaceous to Paleocene succession forms a doubly vergent wedge floored by a significant accumulation of Triassic evaporites. Associated with such accumulation, salt bodies occur and some crop out. The gravity signal associated with these bodies features short-wavelength gravity lows (Santolaria et al., 2016) (Figure 5c, labeled GS2). South of it, a prominent gravity low (−30 mGal, Figure 5c, labeled TZ1) correlates with the Barbastro-Balaguer Anticline interpreted as a salt-cored duplex system (Santolaria et al., 2020). Further south, the flat-lying Ebro Basin deposits lie over an autochthonous, ca. 1,270 m-thick Lower Triassic to Jurassic succession drilled by the Monzón-1 (Mo-1) exploration well (Lanaja, 1987).

The west-east Otín-Oliana section (Figure 5d) illustrates the along-strike architecture of the Peña Montañesa-Montsec Thrust Sheet and its lateral footwalls. In the footwall of the eastern oblique ramp, deformation of the Ebro Basin deposits is characterized by an antiformal stack detached along the upper Eocene Cardona salt (Oliana anticline) and flanked by Upper Eocene-Lower Oligocene growth strata (Vergés & Muñoz, 1990). West of it, in the hanging wall of the Montsec-Peña Montañesa Thrust, the Jurassic to Upper Cretaceous succession forms a detachment anticline cored by up to 1.5 km thick Triassic evaporites (i.e., the Isona Anticline, Figure 5d). Westward, this succession slightly deepens to the west following the regional plunge, and is overlain by Paleocene to Eocene rocks of the Graus-Tremp Basin, whose maximum thickness is located at the western termination of the Montsec-Peña Montañesa Thrust Sheet. The N-S trending Luzas Fault truncates the whole Jurassic to Eocene succession and is associated with a relative gravity low (Figure 5d, labeled PM1). West of the Montsec Thrust, in the Gavarnie-Sierras Thrust Sheet, several N-S trending structures are cored by Triassic evaporites (Anastasio, 1987, 1992) whose thickness can be determined from their gravity minima (Santolaria et al., 2016). These structures include diapirs (as the Clamosa dome), detachment anticlines, whether buried (Olsón anticline, Soto & Casas-Sainz, 2001) or not (Balzes anticline, Rodríguez-Pintó et al., 2016), and fault-propagation folds (Boltaña anticline, Muñoz et al., 2013). The described structural units thrust over autochthonous Ebro Basin deposits which, in their turn, overlain a westward deepening basement.

5. Map View and Subsurface Distribution of Middle-Upper Triassic Evaporites in the South Pyrenean Central Salient

Correlation between the presence of salt (or other evaporites) at depth and the gravity lows of a residual Bouguer anomaly stands as a qualitative exercise that yields to draft the potential distribution of salt accumulations. In the SPCS, salt bodies may include, as the Upper Triassic rocks do, a vast catalog of other lithologies as carbonates, shales, volcanic rocks and even high density evaporites such as anhydrites. And, in the South Pyrenean Triangle Zone, evaporites are interbedded with non-evaporitic units. The "dirty" nature of these evaporitic units has been used as a counterargument to invalidate the gravity method as an approach to investigate the distribution of evaporite accumulations in the subsurface. But, both in the SPCS and the South Pyrenean Triangle Zone, there is an obvious correlation: where there are significant accumulations of Triassic or Eocene-Oligocene evaporites gravity anomalies drop and describe gravity lows (e.g., Santolaria et al., 2016, 2020). Exposed diapirs in the western termination of the SPCS (Figure 4c, see anomaly GS1) are good examples. Such correlation also works for salt cored anticlines as the ones found west of anomaly GS1 (Figure 4c), the Isona anticline (Figure 5d) or the South Pyrenean Triangle Zone (Figure 4c, see anomaly TZ1). So, turning the argument around, if the residual Bouguer anomaly maps show gravity highs it is unlikely that there are accumulated evaporites in the subsurface. What about those cropping out evaporitic bodies which are not associated to gravity lows? In these cases, there is not always a direct correlation between accumulation of salt (or, again, other evaporites) at depth in relation to cropping out salt bodies. Few examples in the SPCS are some outcrops along the Nogueras Zone or the Sierras Marginales unit. They could correspond to squeezed salt bodies where just high density rocks remains (salt is gone) or they also could be topped or flanked by relatively low-density rocks, or unconsolidated sediments that may mask the gravity signal produced by evaporites, as for example, in Tunisia, where deep seated diapirs correlate with positive gravity anomalies if hosted by Miocene and Plio-Quaternary deposits (Amiri et al., 2011; Benassi et al., 2006; Hamdi-Nasr et al., 2009) or negative anomalies if basement rocks somehow flank the diapiric bodies (Arfaoui et al., 2011). Therefore, knowledge of the density of other tectonostratigraphic units, different from the evaporites, is key to reduce uncertainties in this qualitative correlation. In any case, to get a quantitative correlation between gravity anomalies and the existence of evaporites at depth, we need gravity modeling.

Gravity forward modeling of the cross-sections gives structural meaning to gravity anomalies and therefore yields further interpretations enabling to delimit the distribution of Triassic evaporites (Figure 6). In those areas where the structural configuration is well constrained by seismic and exploration wells there is not much room for additional reinterpretation of the structural architecture, but there is room for constraining the geometry of evaporite accumulation since salt bodies are poorly imaged by the seismic data in most orogenic settings. In the following, we investigate the distribution of Triassic evaporites and compare our results with previous interpretations. Please note that the cross-sections we present in this work are mainly based on surface geology, seismic interpretation, and exploration wells data, as the other previous cross-sections that we discussed here are (Figure 2). But, in our case, we include the gravity anomalies as an additional constraint.

The eastern half of this salient is characterized by relatively high gravity values punctuated by low anomalies (Figure 4). These low gravity anomalies correspond to (Figure 6): (a) salt accumulations along the Nogueras Zone, (b) a salt body surrounding the Roca Narieda structure (Figure 6) that links with a salt accumulation at the northeasternmost corner of the SPCS, and the salt-cored Isona anticline. Thus, gravity data rules out the possibility of a large, c. 18 km-long and 2 to 4 km-thick accumulation of salt underneath the Organya Basin as recently proposed by Burrel et al. (2021) (Figure 2b). The data presented here is more consistent with a thin residual Triassic salt or a salt weld flooring the basin as proposed by Muñoz (1992), Berástegui et al. (1993), Muñoz et al. (2018) (Figures 2c, 2d, and 5a) and Casini et al. (2023) (their cross-section OB4) and García-Senz et al. (2024) (cross-section in their Figure 3). These Triassic evaporites progressively thickens to the west (Figures 2e, 2g, and 5b).

The most prominent gravity low in the Cotiella-Bóixols Thrust Sheet (CB2) is located between the Organyà and Cotiella basins. Like the Organyà Basin, the Cotiella one coincides with a gravity high, which is consistent with the scarce remnants of Triassic evaporites flooring the depocenters of the exposed minibasins (Kalifi et al., 2023; López-Mir et al., 2014, 2015). The eastern termination of the CB2 gravity low (Figure 4c) coincides with the salt structures related with the Sopeira, Sant Gervàs, and Aulet sub-basins (Gannaway et al., 2022; Saura et al., 2016; Figure 2e) (Figures 5b and 6). This large gravity low extends further south and west into the synorogenic, upper Santonian to Campanian turbidites. This raises a question regarding the possible contribution of a thick succession

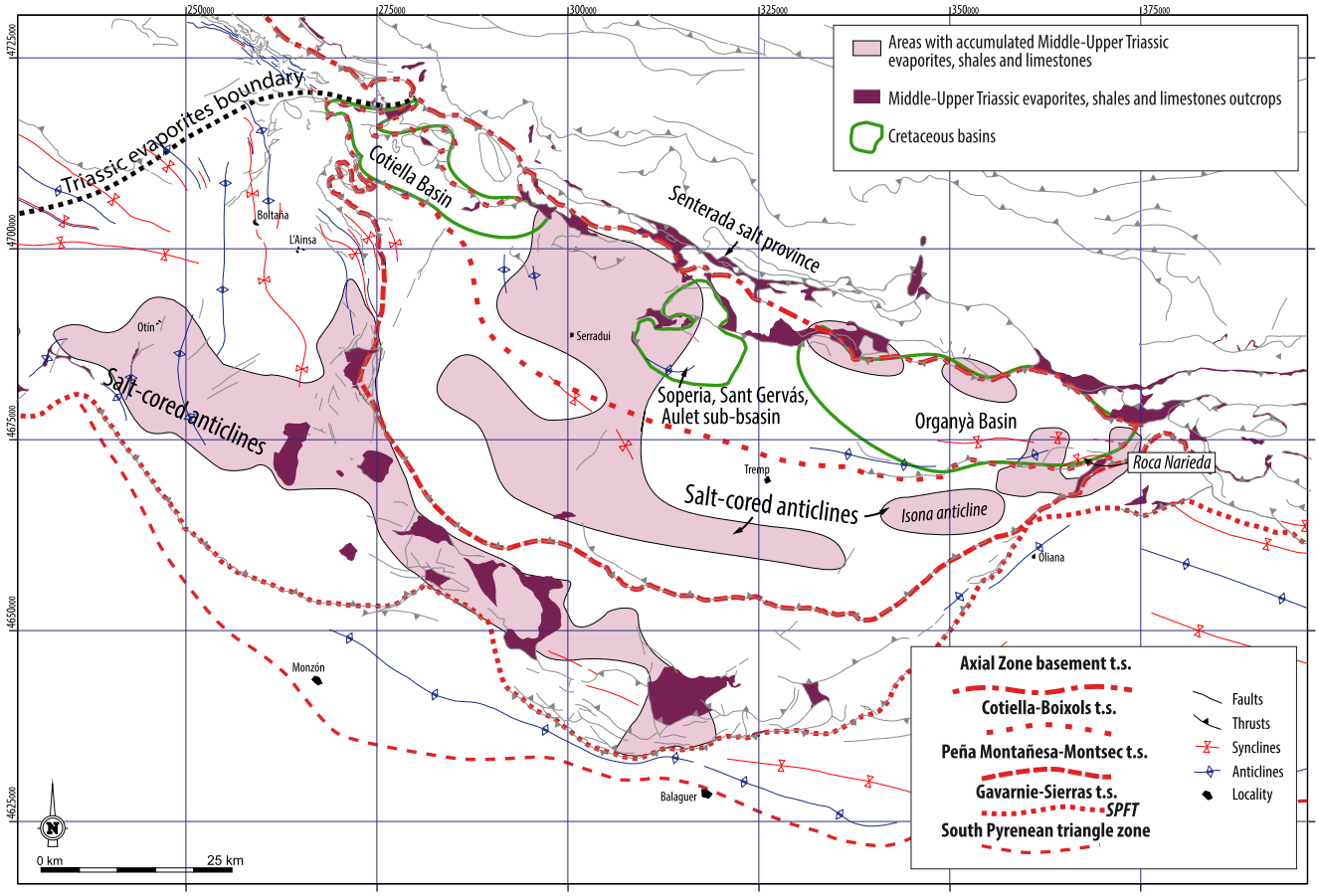

Figure 6. Distribution of Triassic evaporites in the South Pyrenean Central Salient after residual Bouguer anomaly interpretation and gravity forward modeling.

of these turbidites to the gravity low with respect to a possible preserved thick salt underneath. Even though considering a low density for those turbidites (ca. 2.5 g/cm^3), there is still a need for a low-density body, being the Middle-Upper Triassic evaporites the best candidate. Our interpretation involved a less advanced Ribagorza basement Thrust Sheet with respect to former interpretations (Clariana et al., 2022; García-Senz, 2002; Muñoz et al., 2018; Figures 2f and 2g). The gap between both interpretations is therefore filled with Triassic evaporites (compare Figures 2f and 2g and the Cinca-Isábena section, Figure 5c).

Gravity data reveal a succession of gravity highs along the Montsec Thrust, only interrupted by a relative gravity low in the center of the structure (approximately between PM2 and GS3 gravity highs) and the gravity low related with the Clamosa dome. To the east, the gravity data indicate low volumes of Middle-Upper Triassic evaporites at depth supporting the interpretations of, for example, Muñoz (1992) and Berástegui et al. (1993) (Figure 2h), which was adopted in our work (Figure 5a, section Noguera-Pallaresa). To the center of the SPCS, the data are not consistent with recent interpretations which have suggested over 2 km of Triassic salt beneath the Montsec Thrust (Figure 2i, Burrel & Teixell, 2021; Hudec et al., 2021) but neither points out to the absence of evaporites (e.g., Teixell & Muñoz, 2000; Figure 2). An intermediate interpretation considering a triangular accumulation in the footwall of the Montsec Thrust is provided here (Figure 5b). To the west, the topographically prominent Montsec Thrust front is unconformably overlain by Oligocene conglomerates and only some scattered outcrops of the Triassic to Paleocene rocks of its hanging wall appear. These outcrops, few seismic profiles and Benabarre-1 (Be-1) and Benabarre-2 (Be-2) exploration wells together with a gravity maximum (Figure 5b, labeled PM2) allows us to reinterpret the Montsec thrust front as a pop-up structure. This interpretation differs from previous interpretations where the Montsec is interpreted as a south-directed thrust (Figure 2j, Barnolas et al., 1994; Gessal, 2010; Martínez Peña, 1991) eventually truncated by diapiric bodies belonging to the Gavarnie-Sierras Thrust Sheet (Cámara & Flinch, 2017; Soto et al., 2002; Figure 2k).

Santolaria et al. (2014, 2016, 2020) assessed the gravity signal of the surface and subsurface of the western half of the Gavarnie-Sierras Thrust Sheet, paying special attention to the distribution of Triassic and Eocene-Oligocene evaporites. From seismic interpretation and gravity modeling and inversion, they characterized the distribution of the Eocene-Oligocene autochthonous Ebro Basin deposits (Santolaria et al., 2020), and the height and geometry of several salt bodies and their connection at depth (Santolaria et al., 2014, 2016). In the central to eastern Gavarnie-Sierras Thrust Sheet, seismic coverage is very scarce and seismic image quality very poor. Besides, there are no exploration wells. Thus, the question arises on how to fill the space between the topmost structure, well-exposed at surface, and the top of the basement, located between 2.5 and 5 km underneath. This is still an ongoing debate. Possibilities include a deformed (Figure 2l, e.g. Senz & Zamorano, 1992; Teixell & Muñoz, 2000) or undeformed (e.g., Martínez-Peña & Pocoví, 1988; Figure 2m) Ebro Basin autochthonous sequence or a repetition of the Gavarnie-Sierras Thrust Sheet units (e.g., Berástegui et al., 1993; Muñoz, 1992; Muñoz et al., 2018; Figure 2h). Along the Cinca-Isábena and specially in the Noguera-Ribagorzana section, density values indicate that Eocene to Oligocene terrigenous rocks are present beneath the Gavarnie-Sierras thrust unit (Santolaria et al., 2020). The interpretation presented here (Figure 5b) suggests that there is a c. 2.5 km thick succession of Eocene-Oligocene Ebro Basin sediments beneath this thrust sheet, in agreement with Martínez-Peña and Pocoví (1988). But, to the east, along the Noguera-Ribagorzana section, gravity modeling points out to thrust stacking of the Ebro Basin deposits as proposed by Senz and Zamorano (1992) and Teixell and Muñoz (2000). To the east, in the Noguera-Pallaresa section and as one of the most valuable contributions of the gravity map and the gravity-constrained sections is that gravity values rule out the existence of a significant amount of Triassic evaporites at depth, in contrast to existing interpretations (Hypothesis 1 in Burrel & Teixell, 2021; Garrido-Megías & Ríos, 1972; Figure 2i). In the interpretation presented here, Triassic evaporites are likely to be restricted to thin remnants along the thrust-fault detachments (Figure 5a).

All in all, gravity models in combination to the residual Bouguer anomaly maps enable us to provide a strong constraint on the distribution of the Middle-Upper Triassic evaporites and shales whose implications are discussed in the following section. This map represents an extra input to consider when constructing sections across the SPCS. It also proves that despite there is a straight correlation between known accumulation of evaporites and gravity lows, Triassic salt outcrops do not necessarily correlate with in-depth salt accumulations (Cámara & Flinch, 2017) as it is the case of several salt bodies along the Senterada Diapir Province, or the eastern half of the Gavarnie-Sierras Thrust Sheet (Figure 6).

6. Implications of the Distribution of Triassic Evaporites in the SPCS

In the SPCS, the Middle-Upper Triassic evaporites and shales crop out as a strongly deformed tectonic mélange (e.g., Saura et al., 2016) which hinders a reliable calculation of its original thickness. Based on outcrops from the Sierras Marginales unit and the Nogueras Zone, Salvany and Bastida (2004) suggested an original thickness of up to 400 m for the Upper Triassic succession, while more recently Ortí et al. (2017) increase this value up to c. 1,000 m. The evaporitic nature of Middle-Upper Triassic rocks, and therefore their low-strength, together with its uneven areal and thickness distribution, that may vary from few meters to four times the maximum suggested original thickness, indicate these rocks have been mobilized, migrated, and accumulated over the evolution of the basins involved into the Pyrenees. Such halokinetic processes have been observed and described in relation to both the Mesozoic extension and the Pyrenean orogeny (Brinkmann & Lögters, 1968; Burrel & Teixell, 2021; Burrel et al., 2021; Cámara & Flinch, 2017; Canérot et al., 2005; Cofrade et al., 2023; Garcia-Senz et al., 2024; McClay et al., 2004; Rios, 1948; Saura et al., 2016; Serrano & Martínez del Olmo, 1990; Wagner et al., 1971, among others). In addition, there is evidence of salt extrusion and erosion during Pyrenean rift and post-rift stages, which makes the calculation of the original volume of salt even more challenging.

The map view distribution of Triassic evaporites and shales in the SPCS (Figure 6) still stands as a qualitative, but strongly constrained, approach for the actual, quantitative distribution of these rocks. It is only along the modeled sections where we can provide a reliable in-depth distribution of these lithologies. To quantify the volumetric distribution of Triassic evaporites and help to constrain the minimum initial volume of them, 3D gravity modeling (inversion) is needed. Our work provides the foundations to do that. For now, we can discuss the implication of the qualitative (in map view) and quantitative (along the presented sections) distribution of Triassic evaporites regarding the evolutionary context of the SPCS. As pointed out, upon the distribution of Upper Triassic evaporites

and shales we can distinguish (a) few isolated Triassic salt accumulations and a large one in the Cotiella-Bóixols Thrust Sheet, (b) salt-cored anticlines in the Peña Montañesa-Montsec Thrust Sheet, and (c) salt accumulated in the Gavarnie-Sierras Thrust Sheet, especially in its central-western half.

North of the studied area, the Cotiella-Bóixols Thrust Sheet includes three pre-contractional shifting depocenters (García-Senz & Muñoz, 2019a, 2019b): the Organyà Basin (latest Tithonian-middle Albian), Sopeira-Sant Gervàs-Aulet sub-basins (middle Albian-lower Cenomanian), and Cotiella Basin (Coniacian-early Santonian). First one developed during the Early Cretaceous rifting. The other two resulted from postrift gravitational-induced extensional collapse and related salt withdrawal, raft tectonics, and formation of minibasins or rollovers in the North Iberian rifted margin (López-Mir et al., 2014, 2015; McClay et al., 2004; Saura et al., 2016). Early Cretaceous diapirism has been recognized along the northern edge of the Organyà Basin (García-Senz & Muñoz, 2019a), in the so-called Senterada salt province (Figure 6), where Triassic salts were exposed or close to the surface (Burrel et al., 2021; Saura et al., 2016). Later on, and to the west, the Sopeira sub-basin subsided and the evacuated Triassic evaporites fed a diapiric structure to the north. In addition, younger minibasins (Sant Gervás, Faiada, Monteberri) also developed further north by downbuilding (Gannaway et al., 2022; Saura et al., 2016). Further east, in the Cotiella Basin several salt-related isolated basins have been interpreted to develop due to gravity-driven extension during Coniacian to Early Santonian. In between them, diapiric bodies formed and were exposed at the surface (Kalifi et al., 2023; López-Mir et al., 2015). Between the Sopeira Basin and the Cotiella Basin, there are no prominent pre-orogenic Cretaceous basins. Such spatial gap coincides, nowadays, with the prominent salt accumulation in the Cotiella-Bóixols Thrust Sheet. This indicates that this salt accumulation may be an inherited feature likely reworked during the Pyrenean orogeny. Basin subsidence over salt triggered salt withdrawal that fed this salt accumulation, first from the east (Organyà and Sopeira basins, Albian to early Santonian) and second from the west (Cotiella Basin, Coniacian to Early Santonian). This inherited Triassic evaporites accumulation likely hosted the several-km thick depocenter of syn-orogenic turbidites depicted in the Cinca-Isábena section (García-Senz, 2002; Muñoz et al., 2018). All of the above-mentioned basins formed part of the salt-bearing North Iberian rifted margin. Inversion of these salt-detached rifted margins leads to an intricate distribution of remobilized salt whose pre-orogenic distribution may be completely obliterated during mountain building, to the point that salt décollements are almost fully expelled to the surface and eroded and just the remnants of them are preserved, as observed, for example, in the Northern Calcareous Alps of Austria (Granado et al., 2019; Strauss et al., 2023), the Betic Cordillera (e.g., Berástegui et al., 1998; Escosa et al., 2018; Pedrera et al., 2020) or in analog models of inverted salt-bearing passive margins (Santolaria et al., 2022) where up to 75% of the original salt is lost by extrusion and erosion after c. 40% of shortening.

South of it, as evidenced by seismic interpretation and gravity modeling (Santolaria et al., 2016; this study), the Montsec-Peña Montañesa shows a high cover to Triassic-salt ratio, while it is remarkably lower (yet variable) in the Sierras Marginales unit, particularly toward the central and western areas. Question arises regarding if these ratios correspond to the original, pre-orogenic to syn-orogenic configuration of the basin or if salt was remobilized before and/or during shortening. Casini et al. (2023) and Burrel and Teixell (2021) postulated a pre-orogenic thickness of Triassic evaporites varying between c. 0.7–1.5 and 2.3 km (Burrel & Teixell, 2021; Casini et al., 2023, respectively) lying over a faulted basement than deepens toward the north. These authors suggest that some of the accommodation space created in the Graus-Tremp Basin resulted from salt withdrawal toward the edges of the basin. Conversely, Hudec et al. (2021) proposed that Triassic salts were deposited in a graben-horst-graben geometry that controlled their thicknesses leading to the existence of a structural high in the center of the basin. In their model, most of the Peña Montañesa-Montsec Thrust Sheet and the Graus-Tremp Basin deposited over thin (few hundreds of meters) Triassic evaporites lying above the horst. North and south of it, two salt provinces, broadly corresponding to the Gavarnie-Sierras and Cotiella-Bóixols Thrust Sheets, formed over thicker salt.

Toward the western half of the SPCS, in the Gavarnie-Sierras Thrust Sheet, where salt accumulations are larger (Figure 6), salt structures mainly developed at the late stages of contractional deformation, during the Oligocene-Early Miocene (e.g., Cofrade et al., 2023; Martínez-Peña & Pocoví, 1988; Pocoví, 1978) yet there are some sedimentological and stratigraphic evidence of growth of salt-inflated ridges from Upper Cretaceous (Ramirez-Perez et al., 2024). There, the syn-orogenic but pre-folding/thrusting sequence in the Gavarnie-Sierras Thrust Sheet (Upper Cretaceous to Cuisian) shows a gentle thinning trend toward the south (e.g., Berástegui et al., 1993; Millán, 1996) and west (e.g., Soto et al., 2002), and no abrupt thickness changes have been described in this area,

even in the vicinities of the major diapirs (e.g., Muñoz et al., 2013, 2018; Soto et al., 2002). In addition, there is not any evidence of piercing of the suprasalt succession by the Triassic salt during the Mesozoic and Early Middle Eocene, and during this time salt tectonics was restricted to salt migration toward the core of detachment folds (e.g., Teixell & Muñoz, 2000). The absence of salt-related structures suggests a relatively thin Triassic evaporite layer. This is because the mobility of the salt décollement decreases with its thickness. Therefore, partly, Triassic evaporites in the Gavarnie-Sierras Thrust Sheet are allochthonous, likely evacuated from the Peña Montañesa-Montsec Thrust Sheet (Santolaria et al., 2016). Therefore, we postulated a relatively original thin Triassic salt in this area rather than thick, autochthonous salt (Burrel & Teixell, 2021; Casini et al., 2023; Garcia-Senz et al., 2024; Hudec et al., 2021), inflated during mountain building. Migration and accumulation of salt in the most frontal areas of salt-floored foreland basins has been described in other orogens as in the Salt Range of Pakistan (Himalayas, e.g. Baker et al., 1988), where Infra-Cambrian salt is approximately five times thicker in the front of the salt-detached foreland basin than in its interior. Or, in the western Betics (Southern Spain), where autochthonous Triassic salt was expelled out and accumulated at the frontal part of the fold-and-thrust belt where it even hosts secondary minibasins (Pedrera et al., 2020). In contractional analog models including tapered cover-décollement sequences, ductile décollements tend to migrate toward thinner cover areas (e.g., Cotton & Koyi, 2000; Muñoz et al., 2024; Santolaria et al., 2022; Smit et al., 2003; Storti et al., 2007), as suggested for the SPCS.

Nowadays distribution of Middle-Upper Triassic evaporites and shales in the SPCS results from the Mesozoic extension and subsequent inversion, during the Pyrenean orogeny, of an area of the salt-bearing Bay of Biscay-Pyrenean Atlantic passive margin. We suggest that evolutionary models of the SPCS and the Southern Pyrenees should consider this distribution as a constraint.

7. Conclusions

Substantially improved and harmonized Bouguer and residual Bouguer anomalies together with seismic and gravity-constrained sections allow to characterize the distribution of Upper-Middle Triassic evaporites and shales along the SPCS and surrounding areas. The observed residual Bouguer anomaly shows an axial long-wavelength asymmetry where higher values dominate along the eastern half. Such asymmetry results from the combination of a shallower basement and a lesser amount of evaporites to the east. Over this regional feature, few to tens km-wide gravity lows represent Triassic evaporite accumulations. To the north of the salient, salt accumulations are located in front of the Nogueras Zone but the most significant one is located to the center-west of the Cotiella-Bòixols Thrust Sheet between Organyà and Cotiella highly subsiding Lower and Upper Cretaceous basins, respectively. To the south, along the Peña Montañesa-Montsec and Gavarnie-Sierras Thrust Sheet, salt cored detachment anticlines are present while the Montsec frontal structure is characterized by very thin or absent Triassic evaporites, except for the Clamosa dome diapir. Finally, the central to western Sierras Marginales unit are interpreted to be a salt inflated area rooting and feeding detachment anticlines, thrusts, diapirs and salt sheets, especially to the west. In addition, gravity anomalies rule out the presence of abundant salt in the eastern part of the Sierras Marginales unit.

All in all, thanks to the combination between residual Bouguer anomaly map analysis and gravity forward modeling we demonstrate the variable distribution of Triassic evaporites and salt related structures in the SPCS. We found that there is a direct correlation of evaporite accumulations, either cropping out or not, and gravity lows. This allows to argue that, in those areas with gravity highs it is unlikely to find large amounts of evaporites underneath. Besides, we want to highlight the fact that outcropping evaporites do not necessarily correlate with at-depth accumulations of them.

Data Availability Statement

Seismic reflection profiles and gravity data for this research are available and freely accessible in the SIGEOF repository, the Geophysical Information System of the IGME (Spanish Geological Survey), and the DIGITAL CSIC repository. To access the data, use the web application (info.igme.es/SIGEOF/) and visit the web page http://hdl.handle.net/10261/254934 or https://doi.org/10.20350/digitalCSIC/14026 (Ayala, Rey-Moral, Rubio Sánchez-Aguililla, et al., 2021).

Acknowledgments
This work is a joint contribution of the IGME-CSIC, Geosciences Barcelona - CSIC and the Institut de Recerca Geomodels (Universitat de Barcelona). This work is part of the project PID2020-114273GB-C22, High-resolution imaging of the crustal-scale structure of the Central Pyrenees and role of Variscan inheritance on its geodynamic evolution (IMAGYN), funded by MICIU/AEI/10.13039/501100011033 and the project PID2020-117598GB-I00, Structure and Deformation of Salt-bearing Rifted Margins (SABREM), funded by MICIU/AEI/11.13039/501110011133 from the Spanish Ministry of Science and Innovation and the "Severo Ochoa" extraordinary grants for excellence IGME-CSIC (AECEX2021). Petroleum Experts are also acknowledged for providing Move software.

References

Aguilar, C., Liesa, M., Castiñeiras, P., & Navidad, M. (2014). Late Variscan metamorphic and magmatic evolution in the eastern Pyrenees revealed by U-Pb age zircon dating. *Journal of the Geological Society*, *171*(2), 181–192. https://doi.org/10.1144/jgs2012-086

AllahTavakoli, Y., Safari, A., Ardalan, A., & Bahrodi, A. (2015). Application of the RTM-technique to gravity reduction for tracking near-surface mass-density anomalies: A case study of salt diapirs in Iran. *Studia Geophysica et Geodaetica*, *59*(3), 409–423. https://doi.org/10.1007/s11200-014-0215-9

Amiri, A., Chaqui, A., Hamdi-Nasr, I., Inoubli, M. H., Ben Ayed, N., & Tlig, S. (2011). Role of preexisting faults in the geodynamic evolution of Northern Tunisia, insights from gravity data from the Medjerda valley. *Tectonophysics*, *506*(1–4), 1–10. https://doi.org/10.1016/j.tecto.2011.03.004

Anastasio, D. J. (1987). *Thrusting, halotectonics and sedimentation in the external Sierra, southern Pyrenees, Spain* (p. 181). Unpublished PhD thesis. The Johns Hopkins University.

Anastasio, D. J. (1992). Structural evolution of the external Sierra, southern Pyrenees, Spain. In S. Mitra & G. W. Fisher (Eds.), *Structural geology of fold and thrust belts* (pp. 239–251). Johns Hopkins Univ. Press.

Ardestani, V. E., Fournier, D., & Oldenburg, D. W. (2022). A localized gravity modeling of the upper crust beneath central Zagros. *Pure and Applied Geophysics*, *179*(6–7), 2365–2381. https://doi.org/10.1007/s00024-022-03065-1

Ardèvol, L., Klimowitz, J., Malagón, J., & Nagtegaal, P. J. C. (2000). Depositional sequence response to foreland deformation in the upper cretaceous of the southern Pyrenees, Spain. *American Association of Petroleum Geologists Bulletin*, *84*(4), 566–587. https://doi.org/10.1306/c9ebce55-1735-11d7-8645000102c1865d

Arfaoui, M., Inoubli, M. H., Tlig, S., & Alouani, R. (2011). Gravity analysis of salt structures. An example from the El Kef-Ouargha region (northern Tunisia). *Geophysical Prospecting*, *59*(3), 576–591. https://doi.org/10.1111/j.1365-2478.2010.00941.x

Ayala, C., Bohoyo, F., Maestro, A., Reguera, M. I., Torne, M., Rubio, F., et al. (2016). Updated Bouguer anomalies of the Iberian Peninsula: A new perspective to interpret the regional geology. *Journal of Maps*, *12*(5), 1089–1092. https://doi.org/10.1080/17445647.2015.1126538

Ayala, C., Rey-Moral, C., Rubio, F., Soto, R., Clariana, P., Martín-León, J., et al. (2021). Gravity data on the central Pyrenees: A step forward to help a better understanding of the Pyrenean structures. *Journal of Maps*, *17*(2), 750–759. https://doi.org/10.1080/17445647.2021.2001386

Ayala, C., Rey-Moral, M. C., Rubio Sánchez-Aguililla, F. M., Martín León, J., Llorente, J. M., González Durán, A., et al. (2021). Gravity data from the GeoPiri3D project (2.5D and 3D characterization of the crustal structure of the Catalan Pyrenees with special attention to granitic bodies and Permocarboniferous volcano-sedimentary basins. https://doi.org/10.20350/digitalCSIC/14026

Bahroudi, A., & Koyi, H. A. (2003). Effect of spatial distribution of Hormuz salt on deformation style in the Zagros fold and thrust belt: An analogue modelling approach. *Journal of the Geological Society*, *160*(5), 719–733. https://doi.org/10.1144/0016-764902-135

Baker, D. M., Lillie, R. J., Yeats, R. S., Johnson, G. D., Yousuf, M., & Hamid Zamin, A. S. (1988). Development of the Himalayan frontal thrust zone: Salt range, Pakistan. *Geology*, *16*(1), 3–7. https://doi.org/10.1130/0091-7613(1988)016<0003:dothft>2.3.co;2

Barnolas, A., & Gil-Peña, I. (2001). Ejemplos de relleno sedimentario multiepisódico en una cuenca de antepaís fragmentada: La Cuenca Surpirenaica. *Boletin Geologico y Minero*, *112*(3), 17–38.

Barnolas, A., Teixell, A., García Senz, J., & Ramirez, J. I. (1994). *Mapa Geológico de España. 1:50000, Hoja 288, Fonz*. IGME.

Beamud, E., Muñoz, J. A., Fitzgerald, P. G., Baldwin, S. L., Garcés, M., Cabrera, L., & Metcalf, J. R. (2011). Magnetostratigraphy and detrital apatite fission track thermochronology in syntectonic conglomerates: Constraints on the exhumation of the South-Central Pyrenees. *Basin Research*, *23*(3), 309–331. https://doi.org/10.1111/j.1365-2117.2010.00492.x

Beaumont, C., Muñoz, J. A., Hamilton, J., & Fullsack, P. (2000). Factors controlling the Alpine evolution of the central Pyrenees inferred from a comparison of observations and geodynamical models. *Journal of Geophysical Research*, *105*(B4), 8121–8145. https://doi.org/10.1029/1999jb900390

Benassi, R., Jallouli, C., Hammami, M., & Turki, M. M. (2006). The structure of Jebel El Mourra, Tunisia: A diapiric structure causing a positive gravity anomaly. *Terra Nova*, *18*(6), 432–439. https://doi.org/10.1111/j.1365-3121.2006.00709.x

Berástegui, X., Banks, C. J., Puig, C., Taberner, C., Waltham, D., & Fernandez, M. (1998). Lateral diapiric emplacement of Triassic evaporites at the southern margin of the Guadalquivir Basin, Spain. *Geological Society, London, Special Publications*, *134*(1), 49–68. https://doi.org/10.1144/gsl.sp.1998.134.01.04

Berástegui, X., Losantos, M., Muñoz, J. A., & Puigdefàbregas, C. (1993). *Tall geologic del Pirineu Central. 1:200,000*. Barcelona, Servei Geològic de Catalunya-Institut Cartogràfic de Catalunya.

Brinkmann, R. V., & Lögters, H. (1968). Diapirs in western Pyrenees and foreland Spain. *American Association of Petroleum Geologists Memoir*, *8*, 275–292.

Burrel, L., & Teixell, A. (2021). Contractional salt tectonics and role of pre-existing diapiric structures in the Southern Pyrenean foreland fold–thrust belt (Montsec and Serres Marginals). *Journal of the Geological Society*, *178*(4). https://doi.org/10.1144/jgs2020-085

Burrel, L., Teixell, A., Gómez-Gras, D., & Coll, X. (2021). Basement-involved thrusting, salt migration and intramontane conglomerates: A case from the southern Pyrenees. *Bulletin de la Societe Geologique de France*, *192*(1), 24. https://doi.org/10.1051/bsgf/2021013

Callot, J. P., Trocmé, V., Letouzey, J., Albouy, E., Jahani, S., & Sherkati, S. (2012). Pre-existing salt structures and the folding of the Zagros Mountains. *Geological Society, London, Special Publications*, *363*(1), 545–561. https://doi.org/10.1144/SP363.27

Calvin, P., Santolaria, P., Casas, A. M., & Pueyo, E. L. (2017). Detachment fold vs. Ramp anticline: A gravity survey in the southern Pyrenean front (external Sierras). *Geological Journal*, *53*(1), 178–190. https://doi.org/10.1002/gj.2884

Cámara, P., & Flinch, J. F. (2017). The southern Pyrenees: A salt-based fold-and-thrust belt. In J. I. Soto, J. Flinch, & G. Tari (Eds.), *Permo-triassic salt provinces of Europe, North Africa and the Atlantic Margins* (pp. 395–415).

Canérot, J., Hudec, M. R., & Rockenbauch, K. (2005). Mesozoic diapirism in the Pyrenean orogen: Salt tectonics on a transform plate boundary. *AAPG Bulletin*, *89*(2), 211–229. https://doi.org/10.1306/09170404007

Carrillo, E., Guinea, A., Casas, A., Rivero, L., Cox, N., & Vázquez-Taset, Y. M. (2020). Tectono-sedimentary evolution of transverse extensional faults in a foreland basin: Response to changes in tectonic plate processes. *Basin Research*, *32*(6), 1388–1412. https://doi.org/10.1111/bre.12434

Casas, A., Kearey, P., Rivero, L., & Adam, C. R. (1997). Gravity anomaly map of the Pyrenean region and a comparison of the deep geological structure of the western and eastern Pyrenees. *Earth and Planetary Science Letters*, *150*(1–2), 65–78. https://doi.org/10.1016/s0012-821x(97)00087-3

Casini, G., Vergés, J., Drzewiecki, P., Ford, M., Cruset, D., Wright, W., & Hunt, D. (2023). Reconstructing the Iberian salt-bearing rifted margin of the southern Pyrenees: Insights from the Organyà Basin. *Tectonics*, *42*(7), e2022TC007715. https://doi.org/10.1029/2022TC007715

Choukroune, P., & ECORS team. (1989). The ECORS Pyrenean deep seismic profile reflection data and the overall structure of an orogenic belt. *Tectonics*, *8*(1), 23–39. https://doi.org/10.1029/tc008i001p00023

Clariana, P., Soto, R., Ayala, C., Casas-Sainz, A. M., Román-Berdiel, T., Oliva-Urcia, B., et al. (2022). Basement and cover architecture in the Central Pyrenees constrained by gravimetric data. *International Journal of Earth Sciences*, *111*(2), 641–658. https://doi.org/10.1007/s00531-021-02137-2

Cofrade, G., Cantarero, I., Gratacós, Ò., Ferrer, O., Ramirez-Perez, P., Travé, A., & Roca, E. (2023). Allochthonous salt advance recorded by the adjacent syn-kinematic sedimentation: Example from the Les Avellanes diapir (South Central Pyrenees). *Global and Planetary Science*, *220*, 104020. https://doi.org/10.1016/j.gloplacha.2022.104020

Cotton, J. T., & Koyi, H. A. (2000). Modeling of thrust fronts above ductile and frictional detachments: Application to structures in the salt range and Potwar plateau, Pakistan. *Geological Society of America Bulletin*, *112*(3), 351–363. https://doi.org/10.1130/0016-7606(2000)112<351:motfad>2.0.co;2

Crameri, F. (2018). *Scientific colour maps*. Zenodo. https://doi.org/10.5281/zenodo.1243862

Dalloni, M. (1913). Stratigraphie et tectonique de la región des Nogueras (Pyrenees centrales). *Bulletin de la Societe Geologique de France*, *4*(13), 243–263.

Davis, D. M., & Engelder, T. (1985). The role of salt in fold-and-thrust belts. *Tectonophysics*, *119*(1–4), 67–88. https://doi.org/10.1016/0040-1951(85)90033-2

Escosa, F. O., Roca, E., & Ferrer, O. (2018). Testing thin-skinned inversion of a prerift salt-bearing passive margin (Eastern Prebetic Zone, SE Iberia). *Journal of Structural Geology*, *109*, 55–73. https://doi.org/10.1016/j.jsg.2018.01.004

Fillon, C., Huismans, R. S., van der Beek, P., & Muñoz, J. A. (2013). Syntectonic sedimentation controls on the evolution of the southern Pyrenean fold-and-thrust belt: Inferences from coupled tectonic-surface processes models. *Journal of Geophysical Research: Solid Earth*, *118*(10), 1–16. https://doi.org/10.1002/jgrb.50368

Ford, M., Masini, E., Vergés, J., Pik, R., Ternois, S., Léger, J., et al. (2022). Evolution of a low convergence collisional orogen: A review of Pyrenean orogenesis. *BSGF - Earth Sciences Bulletin*, *193*, 19. https://doi.org/10.1051/bsgf/2022018

Fullea, J., Fernàndez, M., & Zeyen, H. (2008). FA2BOUG—AFORTRAN 90 code to compute Bouguer gravity anomalies from gridded free air anomalies: Application to the Atlantic-Mediterranean transition zone. *Computers & Geosciences*, *34*(12), 1665–1681. https://doi.org/10.1016/j.cageo.2008.02.018

Gannaway, C. E., Giles, K. A., Muñoz, J., & Rowan, M. G. (2022). Interpreting the nature of the Aulet and Adons diapirs from sedimentologic and stratigraphic analysis of flanking minibasin strata, Spanish Pyrenees, Catalunya, Spain. *Journal of Sedimentary Research*, *92*(3), 167–209. https://doi.org/10.2110/jsr.2021.179

García-Sansegundo, J. (1996). Hercynian structure of the axial zone of the Pyrenees: The Aran valley cross-section (Spain-France). *Journal of Structural Geology*, *18*(11), 1315–1325. https://doi.org/10.1016/s0191-8141(96)00050-8

García-Sansegundo, J., Poblet, J., Alonso, J. L., & Clariana, P. (2011). Hinterland—Foreland zonation of the Variscan orogen in the central Pyrenees: Comparison with the northern part of the Iberian Variscan Massif. *Geological Society, London, Special Publications*, *349*(1), 169–184. https://doi.org/10.1144/sp349.9

García-Senz, J. (2002). *Cuencas extensivas del cretácico inferior en los Pirineos centrales, formación y subsecuente inversión* (p. 310). PhD Thesis. Universitat de Barcelona.

García-Senz, J., López-Mir, B., Robador, A., Dinarès-Turell, J., & Pedrera, A. (2024). Translation, collision and vertical-axis rotation in the Organyà and Montsec minibasins (South-Central Pyrenees, Spain). *Basin Research*, *36*(1), e12846. https://doi.org/10.1111/bre.12846

García-Senz, J., & Muñoz, J. A. (2019a). The late Albian to middle Cenomanian Aulet and las Aras basins. In C. Quesada & J. Oliveira (Eds.), *Martín-Chivelet J, et al. Late cretaceous post-rift to convergence in Iberia, The geology of Iberia: A geodynamic approach* (pp. 320–324). Regional Geology Reviews. Springer International Publishing.

García-Senz, J., & Muñoz, J. A. (2019b). South central Pyrenees: The Organyà rift basin. In C. Quesada & J. Oliveira (Eds.), *Martín-Chivelet J, et al. The late Jurassic–early cretaceous rifting, the geology of Iberia: A geodynamic approach* (pp. 169–249). Regional Geology Reviews. Springer International Publishing. https://doi.org/10.1007/978-3-030-11295-0_5

Garrido-Megías, A. (1973). *Estudio geológico y relación entre tectónica y sedimentación del Secundario y Terciario de la vertiente meridional pirenaica en su zona central (Provincias de Huesca y Lérida)* (p. 395). PhD thesis. Univ. de Granada.

Garrido-Megías, A., & Ríos, L. M. (1972). Síntesis geológica del Secundario y Terciario entre los ríos Cinca y Segre (Pirineo Central de la vertiente sur pirenaica), provincias de Huesca y Lérida. *Bol. Geol. Min. Esp.*, *83*, 1–47.

Gessal. (2010). Selección y caracterización de áreas y estructuras geológicas favorables para el almacenamiento geológico de CO_2 en España. Instituto Geológico y Minero de España y Reestructuración minería reactivación comarcas. PE-GE-08-GEOL-02-00.

Granado, P., Roca, E., Strauss, P., Pelz, K., & Muñoz, J. A. (2019). Structural styles in fold-and-thrust belts involving early salt structures: The Northern Calcareous Alps (Austria). *Geology*, *47*(1), 51–54. https://doi.org/10.1130/g45281.1

Hamdi-Nasr, I., Inoubli, M. H., Ben Salem, A., Tlig, S., & Mansouri, A. (2009). Gravity contributions to the understanding of salt tectonics from the Jebel Cheid area (dome zone, Northern Tunisia). *Geophysical Prospecting*, *57*(4), 719–728. https://doi.org/10.1111/j.1365-2478.2009.00788.x

Hammer, S. (1939). Terrain corrections for gravimeter stations. *Geophysics*, *4*(3), 184–194. https://doi.org/10.1190/1.1440495

Hindle, D., Besson, O., & Burkhard, M. (2000). A model of displacement and strain for arc-shaped mountain belts applied to the Jura arc. *Journal of Structural Geology*, *22*(9), 1285–1296. https://doi.org/10.1016/s0191-8141(00)00038-9

Hindle, D., & Burkhard, M. (1999). Strain, displacement and rotation associated with the formation of curvature in fold belts; the example of the Jura arc. *Journal of Structural Geology*, *21*(8), 1089–1101. https://doi.org/10.1016/s0191-8141(99)00021-8

Hinze, W. J., von Frese, R. R. B., & Saad, A. H. (Eds.) (2013)., *Gravity and magnetic exploration principles, practices, and applications*. Cambridge University Press. https://doi.org/10.1017/CBO9780511843129

Hudec, M. R., Dooley, T. P., Burrel, L., Teixell, A., & Fernandez, N. (2021). An alternative model for the role of salt depositional configuration and preexisting salt structures in the evolution of the Southern Pyrenees, Spain. *Journal of Structural Geology*, *146*, 104325. https://doi.org/10.1016/j.jsg.2021.104325

Izquierdo-Llavall, E., Ayala, C., Pueyo, E. L., Casas-Sainz, A. M., Oliva-Urcia, B., Rubio, F., et al. (2019). Basement-cover relationships and their along-strike changes in the linking zone (Iberian range, Spain): A combined structural and gravimetric study. *Tectonics*, *38*(8), 2934–2960. https://doi.org/10.1029/2018tc005422

Jallouli, C., Chikhaoui, M., Braham, A., Turki, M. M., Mickus, K., & Benassi, R. (2005). Evidence for Triassic salt domes in the Tunisian Atlas from gravity and geological data. *Tectonophysics*, *396*(3–4), 209–225. https://doi.org/10.1016/j.tecto.2004.12.003

Kalifi, A., Ribes, C., Dietrich, P., Dujoncquoy, E., Muñoz, J.-A., Callot, J.-P., & Ringenbach, J.-C. (2023). Facies distribution along salt walls: The upper cretaceous mixed siliciclastic-carbonate deposits of the Cotiella minibasins (Southern Pyrenees, Spain). *Marine and Petroleum Geology*, *147*, 105989. https://doi.org/10.1016/j.marpetgeo.2022.105989

LaFehr, T. R. (1991). Standardization in gravity reduction. *Geophysics*, *56*(8), 1170–1178. https://doi.org/10.1190/1.1443137

Lanaja, J. M. (1987). *Contribución de la Exploración Petrolífera al Conocimiento de la Geología de España* (p. 465). Instituto. Geológico y Minero de España.
Letouzey, J., Colleta, B., Vially, R., & Chermette, J. C. (1995). Evolution of salt-related structures in compressional settings. In M. P. A. Jackson, D. G. Roberts, & S. Snelson (Eds.), *Salt tectonics, a global perspective* (pp. 41–60). AAPG.
Longman, I. M. (1959). Formulas for computing the tidal accelerations due to the moon and the sun. *Journal of Geophysical Research*, *64*(12), 2351–2355. https://doi.org/10.1029/jz064i012p02351
López-Mir, B., Muñoz, J. A., & García-Senz, J. (2015). Extensional salt tectonics in the partially inverted Cotiella post-rift basin (South-Central Pyrenees): Structure and evolution. *International Journal of Earth Sciences*, *104*(2), 419–434. https://doi.org/10.1007/s00531-014-1091-9
López-Mir, B., Muñoz, J. A., & García-Senz, J. G. (2014). Restoration of basins driven by extension and salt tectonics: Example from the Cotiella Basin in the central Pyrenees. *Journal of Structural Geology*, *69*(PA), 147–162. https://doi.org/10.1016/j.jsg.2014.09.022
Luján, M., Storti, F., Balanyá, J.-C., Crespo-Blanc, A., & Rossetti, F. (2003). Role of décollement material with different rheological properties in the structure of the Aljibe thrust imbricate (Flysch trough, Gibraltar arc): An analogue modelling approach. *Journal of Structural Geology*, *25*(6), 867–881. https://doi.org/10.1016/s0191-8141(02)00087-1
Martínez Peña, B. (1991). *La estructura del límite occidental de la unidad surpirenaica central* (p. 380). PhD thesis. Univ. de Zaragoza.
Martínez-Peña, B., & Pocoví, A. (1988). El amortiguamiento frontal de la estructura de la cobertera Surpirenaica y su relación con el anticlinal de Barbastro-Balaguer. *Acta Geológica Hispánica*, *23*, 81–94.
Martínez-Peña, B., & Casas-Sainz, A. (2003). Cretaceous–tertiary tectonic inversion of the Cotiella Basin (southern Pyrenees, Spain). *International Journal of Earth Sciences*, *92*(1), 99–113. https://doi.org/10.1007/s00531-002-0283-x
Mattauer, M. (1968). Les traits structuraux essentiels de la chaîne pyrénéenne. *Revue de Geographie Physique et de Geologie Dynamique*, *10*(1), 3–12.
McClay, K., Muñoz, J. A., & García-Senz, J. (2004). Extensional salt tectonics in a contractional orogen: A newly identified tectonic event in the Spanish Pyrenees. *Geology*, *32*(9), 737–740. https://doi.org/10.1130/g20565.1
Meigs, A. J., & Burbank, D. W. (1997). Growth of the South Pyrenean orogenic wedge. *Tectonics*, *16*(2), 239–258. https://doi.org/10.1029/96tc03641
Mencos, J., Carrera, N., & Muñoz, J. A. (2015). Influence of rift basin geometry on the subsequent postrift sedimentation and basin inversion: The Organyà Basin and the Bóixols thrust sheet (south central Pyrenees). *Tectonics*, *34*(7), 1452–1474. https://doi.org/10.1002/2014TC003692
Millán, H. (1996). *Estructura y cinemática del frente de cabalgamiento Surpirenaico, Sierras Exteriores aragonesas* PhD thesis. Universidad de Zaragoza.
Millán, H., Pueyo, E. L., Aurell, M., Luzón, A., Oliva-Urcia, B., Martínez Peña, M. B., & Pocoví, A. (2000). Actividad tectónica registrada en los depósitos terciarios del frente meridional del Pirineo central. *Revista de la Sociedad Geologica de Espana*, *13*(2), 117–138.
Moritz, H. (1980). Geodetic reference system 1980. *Bulletin Geodesique*, *54*(3), 395–405. https://doi.org/10.1007/bf02521480
Muñoz, J. A. (1992). Evolution of a continental collision belt: ECORS-pyrenees crustal balanced section. In K. R. McClay (Ed.), *Thrust tectonics* (pp. 235–246). Chapman and Hall.
Muñoz, J. A., Beamud, E., Fernández, O., Arbués, P., Dinares-Turell, J., & Poblet, J. (2013). The Ainsa fold and thrust oblique zone of the central Pyrenees: Kinematics of a curved contractional system from paleomagnetic and structural data. *Tectonics*, *32*(5), 1142–1175. https://doi.org/10.1002/tect.20070
Muñoz, J. A., Ferrer, O., Gratacós, O., & Roca, E. (2024). The influence of the geometry of salt detachments on thrust salient development: An analogue modelling approach based on the South-Central Pyrenean thrust salient. *Journal of Structural Geology*, *180*, 105078. https://doi.org/10.1016/j.jsg.2024.105078
Muñoz, J. A., Mencos, J., Carrera, N., Gratacós, O., Ferrer, O., & Fernández, O. (2018). The structure of the south-central-Pyrenean fold and thrust belt as constrained by subsurface data. *Geológica Acta*, *16*(4), 439–460. https://doi.org/10.1344/GeologicaActa2018.16.4.7
Mutti, E., Séguret, M., & Sgavetti, M. (1988). Sedimentation and deformation in the tertiary sequences of the southern Pyrenees. In *American association of petroleum geologists Mediterranean basins Conference* (Vol. 7, p. 169). Field Trip Guidebook.
Nettleton, L. L. (1968). Gravity anomalies over salt diapirs, northern Spain. *Geological Society of America Special Paper*, *88*, 75–82. https://doi.org/10.1130/spe88-p75
Nijman, W. (1998). Cyclicity and basin analysis axis shift in a piggyback basin: Towards modelling of the Eocene Tremp-Ager basin, south Pyrenees, Spain. In A. Mascle, C. Puigdefàbregas, H. P. Luterbacher, & M. Fernández (Eds.), *En: Cenozoic foreland basins of western Europe* (Vol. 134, pp. 135–162). Geological Society Special Publications.
Ortí, F., Pérez-López, A., & Salvany, J. M. (2017). Triassic evaporites of Iberia: Sedimentological and palaeogeographical implications for the western Neotethys evolution during the middle Triassic–Earliest Jurassic. *Palaeogeography, Palaeoclimatology, Palaeoecology*, *471*, 157–180. https://doi.org/10.1016/j.palaeo.2017.01.025
Pedrera, A., Ruiz-Constán, A., García-Senz, J., Azor, A., Marín-Lechado, C., Ayala, C., et al. (2020). Evolution of the South-Iberian paleomargin: From hyperextension to continental subduction. *Journal of Structural Geology*, *138*, 104122. https://doi.org/10.1016/j.jsg.2020.104122
Piña-Varas, P., Soto, R., Clariana, P., Ayala, C., Rubio, F. M., Ledo, J. J., et al. (2023). High-resolution scan of the Pyrenean crustal structure combining magnetotelluric and gravity data. *Tectonophysics*, *864*, 230022. https://doi.org/10.1016/j.tecto.2023.230022
Pinto, V., & Casas, A. (1996). An interactive 2D and 3D gravity modeling program for IBM-compatible personal computers. *Computers & Geosciences*, *22*(5), 535–546. https://doi.org/10.1016/0098-3004(95)00125-5
Pinto, V., Casas, A., Rivero, L., & Lázaro, R. (2002). Modelización Gravimétrica 3D del diapiro de Cardona, Cuenca del Ebro (NE de España). *Acta Geologica Hispanica*, *37*(4), 273–284.
Plata, J. L. (2014). *Manual program CCT BLOQUES*. Unpublished Report Área Geofísica. IGME.
Poblet, J. (1991). *Estructura herciniana i alpina del Vessant sud de la zona Axial del Pirineu Central* (p. 604). Unpublished PhD Thesis. Univ. of Barcelona.
Pocoví, A. (1978). *Estudio geológico de las Sierras Marginales Catalanas (Prepirineo de Lérida)* (p. 218). PhD thesis. Univ. of Barcelona.
Pueyo, E. L., Izquierdo-Llavall, E., Rodríguez-Pintó, A., Rey-Moral, C., Oliva-Urcia, B., Casas, A. M., et al. (2016). Petrophysical properties in the Iberian range and surrounding areas (NE Spain): 1-density. *Journal of Maps*, *12*(5), 836–844. https://doi.org/10.1080/17445647.2015.1084545
Pueyo, E. L., Román-Berdiel, T., Calvín, P., Bouchez, J. L., Beamud, E., Ayala, C., et al. (2022). Petrophysical characterization of non-magnetic granites; density and magnetic susceptibility relationships. *Geosciences*, *12*(6), 240. https://doi.org/10.3390/geosciences12060240
Pueyo, E. L., Rubio, F. M., Toro, R., González, A., Llorente, J. M., Ezquerro, L., et al. (2021). Mapa de anomalía de Bouguer del Pirineo Suroccidental. *Geotemas*, *18*, 560.
Puigdefàbregas, C., Muñoz, J. A., & Vergés, J. (1992). In K. R. McClay (Ed.), *Thrusting and foreland basin evolution in the southern Pyrenees. En: Thrust tectonics* (pp. 247–254). Chapman & Hall.

Ramirez-Perez, P., Cofrade, G., Martín-Martín, J. D., & Travé, A. (2024). Stratigraphic evolution of a salt-walled basin: The influence of diapirism and compressional tectonics on the sedimentary record of the Estopanyà syncline (South-Central Pyrenees). *Marine and Petroleum Geology*, *163*, 106715. https://doi.org/10.1016/j.marpetgeo.2024.106715

Ramos, A., García-Zenz, J., Pedrera, A., Ayala, C., Rubio, F., Peropadre, C., & Mediato, J. F. (2022). Salt control on the kinematic evolution of the Southern Basque-Cantabrian Basin and its underground storage systems (Northern Spain). *Tectonophysics*, *822*, 229178. https://doi.org/10.1016/j.tecto.2021.229178

Rios, J. (1948). Diapirismo. *Boletin del Instituto Geologico y Minero de Espana*, *LX*(20), 155–390.

Rodríguez-Pintó, A., Pueyo, E. L., Calvín, P., Sánchez, E., Ramajo, J., Casas, A. M., et al. (2016). Rotational kinematics of a curved fold: The Balzes anticline (Southern Pyrenees). *Tectonophysics*, *677*, 171–189. https://doi.org/10.1016/j.tecto.2016.02.049

Roest, W. R., & Srivastava, S. P. (1991). Kinematics of the plate boundaries between Eurasia, Iberia, and Africa in the North Atlantic from the late cretaceous to the present. *Geology*, *19*(6), 613–616. https://doi.org/10.1130/0091-7613(1991)019<0613:kotpbb>2.3.co;2

Roure, F., Choukroune, P., Berastegui, X., Mufioz, J. A., Villien, A., Matheron, P., et al. (1989). ECORS deep seismic data and balanced cross-sections: Geometric constraints on the evolution of the Pyrenees. *Tectonics*, *8*(1), 41–50. https://doi.org/10.1029/tc008i001p00041

Rudman, A. J., Ziegler, R., & Blakely, R. F. (1977). *Fortran program for generation of earth tide gravity values*. Indiana Geological Survey Occasional Paper.

Salvany, J. M., & Bastida, J. (2004). Análisis litoestrátigráfico del Keuper Surpirenaico central. *Revista de la Sociedad Geológica de España*, *17*, 3–26.

Santolaria, P., Ayala, C., Pueyo, E. L., Rubio, F. M., Soto, R., Calvín, P., et al. (2020). Structural and geophysical characterization of the western termination of the South Pyrenean triangle zone. *Tectonics*, *39*(8), e2019TC005891. https://doi.org/10.1029/2019tc005891

Santolaria, P., Casas, A., Casas-Sainz, A. M., & Soto, R. (2016). Gravimetric modelling to assess salt tectonics in the western end of the south Pyrenean central unit. *Journal of the Geological Society*, *174*(2), 269–288. https://doi.org/10.1144/jgs2016-027

Santolaria, P., Casas-Sainz, A. M., Soto, R., Pinto, V., & Casas, A. (2014). The Naval diapir (Southern Pyrenees): Geometry of a salt wall associated with thrusting at an oblique ramp. *Tectonophysics*, *637*, 30–44. https://doi.org/10.1016/j.tecto.2014.09.008

Santolaria, P., Granado, P., Wilson, E. P., de Matteis, M., Ferrer, O., Strauss, P., et al. (2022). From salt-bearing rifted margins to fold-and-thrust belts. Insights from analog modeling and Northern Calcareous Alps case study. *Tectonics*, *41*(11), e2022TC007503. https://doi.org/10.1029/2022TC007503

Santolaria, P., Izquierdo-Llavall, E., Soto, R., Román-Berdiel, T., & Casas-Sainz, A. (2024). Origin of oblique structures controlled by pre-tectonic thickness variations in frictional and salt-bearing fold-and-thrust belts: Insights from analogue modelling. *Journal of Structural Geology*, *179*, 105042. https://doi.org/10.1016/j.jsg.2023.105042

Sarsar-Naouali, B. S., Inoubli, M. H., Amiri, A., Chaqui, A., & Hamdi, I. (2011). Subsurface geology of the Ariana region (Diapir Zone, northern Tunisia) by means of gravity analysis. *Geophysical Prospecting*, *59*(6), 983–997. https://doi.org/10.1111/j.1365-2478.2011.01004.x

Saura, E., Ardévol, L. I., Teixell, A., & Vergés, J. (2016). Rising and falling diapirs, shifting depocenters and FAP overturning in the cretaceous Sopeira and Sant Gervàs subbasins (Ribagorça basin, Pyrenees). *Tectonics*, *35*(3), 638–662. https://doi.org/10.1002/2015TC004001

Schreurs, G., Hänni, R., & Vock, P. (2001). Four-dimensional analysis of analog models: Experiments on transfer zones in fold and thrust belts. *Geological Society of America*, *193*, 179–190. https://doi.org/10.1130/0-8137-1193-2.179

Séguret, M. (1972). *Etude tectonique des nappes et séries décollées de la partie centrale du versant sud des Pyrénées. Caractère synsédimentaire, rôle de la compression et de la gravité*. PhD thesis. University of Montpellier.

Senz, J. G., & Zamorano, M. (1992). Evolución tectónica y sedimentaria durante el Priaboniense superior-Mioceno inferior, en el frente de cabalgamiento de las Sierras Marginales Occidentales. *Acta Geológica Hispánica*, *27*(1–2), 195–209.

Serrano, A., & Martínez del Olmo, W. (1990). Tectónica salina en el Dominio Cántabro-Navarro: Evolución, edad y origen de las estructuras salinas. In F. Ortí & J. M. Salvany (Eds.), *Formaciones evaporíticas de la Cuenca del Ebro y cadenas periféricas, y de la zona de Levante* (pp. 39–53).

Smit, J. H. W., Brun, J. P., & Soukoutis, D. (2003). Deformation of brittle–ductile thrust wedges in experiments and nature. *Journal of Geophysical Research*, *108*(B10), 2480. https://doi.org/10.1029/2002JB002190

Soto, R., Casas, A. M., Storti, F., & Faccenna, C. (2002). Role of lateral thickness variations on the development of oblique structures at the western end of the South Pyrenean Central Unit. *Tectonophysics*, *350*(3), 215–235. https://doi.org/10.1016/s0040-1951(02)00116-6

Soto, R., & Casas-Sainz, A. M. (2001). Geometría y cinemática de las estructuras norte-sur de la cuenca Aínsa. *Revista de la Sociedad Geologica de Espana*, *14*(3), 199–212.

Soto, R., Clariana, P., Ayala, C., Rey-Moral, C. M., Casas-Sainz, A. M., Román-Berdiel, T., et al. (2022). Assessing the internal uppermost crustal structure of the central Pyrenees by gravity-constrained cross sections. *Tectonics*, *41*(8), e2021TC007009. https://doi.org/10.1029/2021TC007009

Storti, F., Soto Marín, R., Rossetti, F., & Casas-Sainz, A. M. (2007). Evolution of experimental thrust wedges accreted from along-strike tapered, silicone-floored multilayers. *Journal of the Geological Society*, *164*(1), 73–85. https://doi.org/10.1144/0016-76492005-186

Strauss, P., Granado, P., Muñoz, J. A., Böhm, K., & Schuster, R. (2023). The northern calcareous Alps revisited: Formation of a hyperextended margin and mantle exhumation in the northern calcareous Alps sector of the neo-tethys (eastern Alps, Austria). *Earth-Science Reviews*, *243*, 104488. https://doi.org/10.1016/j.earscirev.2023.104488

Talwani, M., Worzel, J. L., & Landisman, M. (1959). Rapid gravity computations for two-dimensional bodies with application to the Mendocino submarine fracture zone. *Journal of Geophysical Research*, *64*(1), 49–59. https://doi.org/10.1029/jz064i001p00049

Teixell, A., & Muñoz, J. A. (2000). Evolución tectono-sedimentaria del Pirineo meridional durante el Terciario: Una síntesis basada en la transversal del río Noguera Ribagorçana. *Revista de la Sociedad Geológica de España*, *13*, 295–316.

Torné, M. (1989). 3D gravimetric modeling in the Catalan sector of the Ebro Basin. *Revista de la Sociedad Geológica de España*, *2*, 133–142.

Torné, M., De Cabissole, B., Bayer, R., Casas, A., Daignières, M., & Rivero, A. (1989). Gravity constraints on the deep structure of the Pyrenean belt along the ECORS profile. *Tectonophysics*, *165*(1–4), 105–116. https://doi.org/10.1016/0040-1951(89)90039-5

Toro, R., Izquierdo-Llavall, E., Casas, A. M., Rubio, F. M., Ayala, C., Martín-León, J., et al. (2021). Harmonization procedure of the western Pyrenees using geological, gravimetric, petrophysical, and seismic data (p. 90). GEOERA 3DGEO-EU, 3D Geomodeling for Europe, project number GeoE.171.005. Retrieved from https://geoera.eu/projects/3dgeo-eu/.Report

Van Hoorn, B. (1971). Sedimentology and paleogeography of an upper cretaceous turbidite basin in the South-central Pyrenees, Spain. *Leidse Geologische Mededelingen*, *45*(1), 73–154.

Vergés, J. (1993). *Estudi geològic del vessant Sud del Pirineu Oriental i Central: Evolució en 3D* (p. 203). PhD thesis. Universitat de Barcelona.

Vergés, J., & Muñoz, J. A. (1990). Thrust sequences in the southern central Pyrenees. *Bulletin de la Société géologique de France*, *6*(2), 265–271. https://doi.org/10.2113/gssgfbull.vi.2.265

Vergés, J., Muñoz, J. A., & Martínez, A. (1992). South Pyrenean fold-and-thrust belt: Role of foreland evaporitic levels in thrust geometry. In K. R. McClay (Ed.), *Thrust tectonics* (pp. 255–264). Chapman and Hall.

Wagner, G., Mauthe, F., & Mensink, H. (1971). Der Salzstock von Cardona in Nordospanien. *Geologische Rundschau*, *60*(3), 970–996. https://doi.org/10.1007/bf02046531

Wilkerson, M. S., Smaltz, S. M., Bowman, D. R., Fischer, M. F., & Higuera-Diaz, I. C. (2007). 2-D and 3-D modeling of detachment folds with hinterland inflation: A natural example from the Monterrey salient, northeastern Mexico. *Journal of Structural Geology*, *29*(1), 73–85. https://doi.org/10.1016/j.jsg.2006.07.010

Won, I. J., & Bevis, M. (1987). Computing the gravitational and magnetic anomalies due to a polygon: Algorithms and fortran subroutines. *Geophysics*, *52*(2), 232–238. https://doi.org/10.1190/1.1442298